Utrecht University

Master's Thesis

THE OBSERVATIONS OF AEOLIAN SEDIMENT TRANSPORT

in the mouth of an excavated foredune notch

Author:
Nora Schuring

Supervisors:
prof. dr. Gerben Ruessink
Jorn Bosma MSc

Utrecht University

Faculty of Geosciences
Department of Physical Geography
Earth Surface and Water

Frontpage image:

Foredune notch (N2) viewing towards the sea

Source: Own collection, 15-10-2022

ABSTRACT

Traditional dune management along low-lying densely populated areas was focussed on stabilizing foredunes for decades. These stabilized foredunes acted as a barrier for aeolian sediment transport from the beach into the backdunes. The biodiversity in the backdunes decreased and the backdunes were no longer able to grow vertically with sea level rise, putting future coastal safety at risk. To tackle this problem, foredune notches were excavated to enhance sediment transport from the beach into the backdunes. The construction of these notches was based on trial-and-error. The dynamic wind phenomena within these notches, nor the related sediment transport, are yet fully understood. In this study, we investigated the aeolian sediment transport in the mouth of an excavated notch. The data was collected during a fieldwork (fall 2022) in the second of five notches (N2) in the Dutch National Park Zuid-Kennemerland, excavated in the 20-m high established foredune in 2012-2013.

A temporal averaging interval of 1-minute is an appropriate interval for this setup with this accuracy (with this instrument set-up), when compromises were made between scatter, trend, and quantity of data. However, the trends at the 5-minutes (and even for 10-seconds) averaging interval do not appear to be substantially different. In this study, wind speed gave a much better the best correlation for sediment flux than the Turbulent Kinetic Energy (TKE). In general, sediment transport rates increased with increasing wind speed. When the wind reached a certain threshold (generally between 3 and 5 m/s), sediment transport started and increased in a roughly linear fashion with wind speed (slope between 15 and 30). The trend line of day 5 (Saltation Intensity [cnts/s] = 15.4 * U[m/s] – 48.3) provided a reasonably accurate prediction for sediment transport on other days but has its limitations. On the other hand, the relationship between TKE and sediment transport rates was scattered and not consistent for different locations and under different wind conditions. There is much scatter and no clear dependency between the coefficient of variation of the wind speed (CVk) and sediment transport. In general, variations in the wind (CVk) also cause fluctuations in sediment transport (CV), but there was much scatter and no clear trend.

Under very oblique winds (> 50 degrees, form south-west in this study) the transport rates were highest at the first erosional wall the wind encounters (southern erosional wall in this study). There, the wind speed was highest, the wind was least turbulent (TKE) and the wind direction was altered most. Oblique winds did not move as a uniform sheet through the notch: it is steered along the southern erosional wall, while in the middle and north of the notch the wind was less steered and became more turbulent. Although the wind became more turbulent and had relatively lower wind speeds (compared to approach wind speed) during very oblique winds (> 50 degrees), it was still realigned to the notch orientation and capable of moving large quantities of sediment. This deviates with literature and may be due to the roundness of the southern erosional wall, making the local orientation more southwest-northeast than west-east (orientation of the notch) allowing very oblique winds from the southwest to enter the notch.

ACKNOWLEDGEMENT

First, I would like to thank my supervisor, Gerben Ruessink, for allowing me to participate in his research project. His regular constructive feedback, as well as his limitless patience, were also highly appreciated. Secondly, I want to express my appreciation to my second supervisor, Jorn Bosma, for sharing his knowledge about the instruments and his expertise in data processing within MATLAB. I kindly thank my field colleagues, Sam and Luna, with whom I spent a wonderful and productive time in Bloemendaal aan Zee and Zandvoort. In addition, I would like to express my gratitude towards the technical team of the Earth Simulation Lab, Arjan van Eijk, Bas van Dam, Joey O'Dell and Marcel van Maarseveen, for their assistance in setting up the instruments and sharing their expertise on running them. Finally, I want to express my appreciation to my parents, my sister, Jacob, Alissa, and friends for all their help and patience during my thesis.

TABLE OF CONTENT

LIST OF FIGURES

TABLES

1. INTRODUCTION

More extreme weather events, along with rising sea levels, have the potential to cause major threats along low-lying densely populated countries, like the Netherlands. Multiple coastal safety policies, including hard and soft measures, have been implemented to protect vulnerable areas against marine flooding during storms. Coastal dunes have various functions for humankind; they are used to produce drink water, serve as important natural environments and act as a natural safety barrier to protect the hinterland against marine flooding (Hillen & Roelse, 1995). Along low-lying densely populated regions ensuring coastal safety is often considered as the most important function of coastal dunes and consequently, management of coastal dunes was focused on it for decades (Arens & Wiersma, 1994; Van der Laan et al., 1997). A common approach was planting vegetation to increase the height and volume of the foredune (Arens & Wiersma, 1994; Nordstrom & Arens, 1998). These high stabilized foredunes are seen as crucial to guarantee protection with rising sea levels and changing storm behavior (Hillen & Roelse, 1995). However, these high foredunes also act as a barrier to the aeolian sand transport from the beach into the backdunes (Petersen et al., 2011). Vegetation is not buried by sand; therefore sand transport is no longer resetting the ecological succession, and as a result the biodiversity in the back dunes reduces (Miller, 2015; Pye et al., 2014; Veer & Kooijman, 1997). In addition, the backdunes are not able to grow vertically with sea level rise, putting future coastal safety at risk (Arens et al., 2013).

There have been various attempts to restore biodiversity in the backdunes. One of the initial attempts was removing the vegetation in the back dunes, thereby "resetting" the ecosystem locally (Jungerius et al., 1995). However, this is not a long-term solution because the same issue arose once the vegetation had enough time to reach the same equilibrium. Another attempt to restore biodiversity was removing vegetation from the foredunes. This resulted in more aeolian sand transport from the beach/foredunes to the back dunes. The biodiversity increased and the hinterland was able to grow in volume and height. Unfortunately, this was only a temporary solution because after a while the vegetation grew back and the aeolian transport decreased (Arens et al., 2004).

Many of the solutions require a lot of maintenance and are only temporary. A better solution should be self-maintaining; in a restored environment with re-established aeolian dynamics this might be the case (Arens & Geelen, 2001). The current Dutch dune management strategy involves excavating foredune notches to connect backdunes to the beach-foredune system (Ruessink et al., 2018). These foredune notches are complicated aeolian landforms with no vegetation, where winds can erode and transport sediment (Hesp & Hyde, 1996; Smyth et al., 2014). They serve as channels for wind-driven sediment transport from the beach to the backdunes (Arens et al., 2013; Ruessink et al., 2018).

In general, long-term the bio-geomorphological succession and dynamics of blowouts are quite well understood. These long-term changes are caused by a series of wind events, each of which contains complex wind phenomena with a high degree of turbulence. However, these unique wind phenomena, as well as their relationship to sediment transport, are not fully understood. In addition, the excavated foredunes notches are largely dependent on trial and error. The dune management can be improved by learning more about the processes within excavated notches and blowouts. Research concerning the relation between wind

(e.g., wind speed, CVk and TKE) and sediment transport in a blowout, had limited data output, the measurements were taken primarily in the back of the blowout (deflation basin and depositional lobe), and were performed under limited wind conditions. Therefore, there are numerous opportunities to conduct new research on this topic. The main goal of this thesis is to improve understanding of aeolian sediment transport rates in the mouth of a foredune notch. This goal can be achieved through the examination of both the correlation between different wind characteristics and sediment transport (such as wind speed and TKE) and the spatial variation of sediment flux in the notch mouth as function of the winds approach angle.

The structure of this thesis is as follows. In chapter 2, an extensive literature review is presented addresses the most important information that currently known (and unknown) about coastal dunes, blowouts/excavated notches, and aeolian transport. This chapter ends with the formulation of the research questions. The following chapter covers the methods of this study by providing details about the fieldwork conducted in the National Park Zuid-Kennemerland (NPZK) near Bloemendaal, the Netherlands, and the subsequent data management. This is followed by three chapters that contain the results, discussion, and conclusions, respectively.

2. BACKGROUND

Coastal dunes will form and act as a natural safety barrier to protect the hinterland along coasts with sufficient sand (Hillen & Roelse, 1995). The most seaward dune row is referred to as the foredune. Blowouts, which are sandy depressions caused by wind erosion, can form within these foredunes (Hesp, 2002).

2.1 FOREDUNES

Foredunes are shore-parallel dune ridges formed by aeolian sand deposition within vegetation. In coastal dune systems, foredunes can be found at the most seaward position, but not all foremost dunes are foredunes. Along coasts where foredunes cannot grow, e.g., due to erosion, other dune types may be present at the most seaward position (Hesp, 2002). Foredunes come in a variety of shapes and sizes, ranging from a height less than one meter to established sand walls with an elevation of 30 meters. The latter can be found at areas where vegetation has been planted on the lee sides of the dunes as part of intensive dune management (Arens et al., 2013; Hesp, 2002), such as along the Dutch coast. Although a wide range of foredune types have been classified, they generally can be classified into two types: incipient foredunes and established foredunes. Within these two types, there are numerous morphological and ecological variations. The abundance of vegetation (the type and density), sufficient sediment available, and adequate wind conditions are the most important factors determining the size, morphology, and dynamics of foredunes (Hesp, 2002).

2.1.1 Incipient foredune

Incipient foredunes (also known as embryo dunes) are new or developing foredunes that form within pioneer plants on the upper beach. Plants tend to enhance aerodynamic roughness, which affects mean wind flow and turbulence. The development is typically initiated when sand is deposited behind a barrier, such as driftwood, (relatively) distinct vegetation clumps, or individual plants. The primary factors influencing morphological development are vegetation species, plant density, wind regime, and sand transport rates (Hesp, 2002; Hesp & Walker, 2012). The incipient dunes will develop at a higher pace when the plant density is high and there is sufficient sediment supply. The interaction of sand supply and vegetation also determines whether they will be eroded or can develop into established foredunes (Hesp, 2002; Zarnetske et al., 2015).

2.1.2 Established foredune

Incipient foredunes can develop into established foredunes. Established foredunes can be distinguished from incipient foredunes by differences in the plant species (often more woody and persistent vegetation), they have a greater height, width, and age, as well as more complex morphology (Hesp, 2002). Wind velocity, beach width and sediment supply are three (of several) factors that influence or control foredune development. The highest foredunes are typically found along erosional coasts where dune heights are artificially raised, for example by nourishments and planting of vegetation to maintain slope stability (Hesp, 2002).

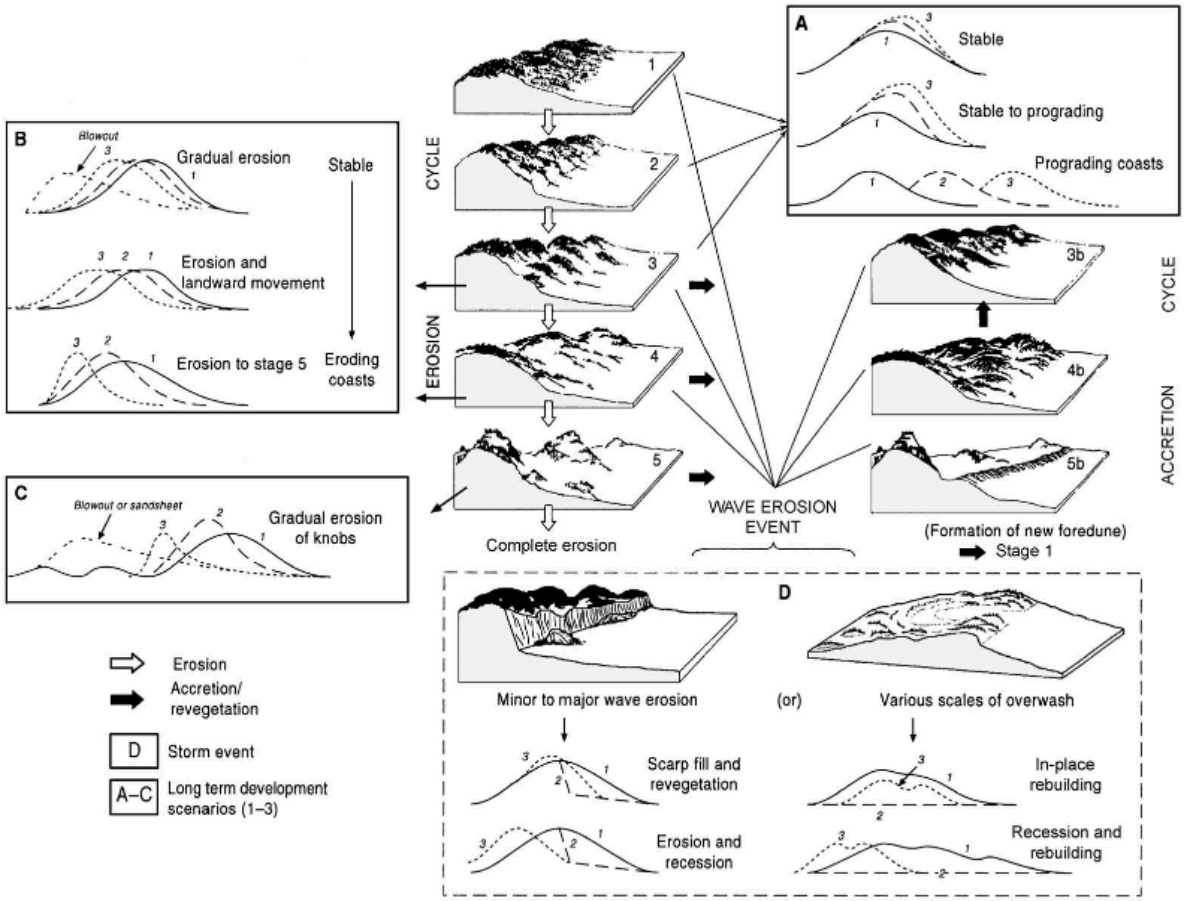

Figure 2.1: Evolutional trends of established foredune morphology. It includes 5 stages for stable (1,2), erosional (3-5) and accreting (3b-5b) dunes. Source: Hesp (2002).

Hesp (2002) classified five stages of established foredune evolution. Stage 1 and 2 are stable foredunes and stage 3-5 are unstable foredunes (Figure 2.1). Foredunes will evolve through an erosion or accretion cycle, depending on the conditions mentioned above. A foredune can evolve from very stable (densely vegetated, straight dune row) into a highly erosional foredune, resulting in, for example, blowouts. When environmental conditions change in favor of a densely vegetated foredune, the erosional process can be reversed into the accretion cycle. Since this thesis will focus on the evolution of (man-made) blowouts inside foredune complexes, phases 3-5 of Hesp (2002) categorization are the most relevant (considering both the erosion and accretion cycles).

2.2 BLOWOUTS

A blowout is a depression formed by local erosion of the wind in a dune (Hesp, 2002). Blowouts can be found in most dune types, including coastal dunes (e.g. foredunes, see 2.1) and desert environments (Hesp & Walker, 2012). A blowout consists of a non-vegetated area called the deflation basin, that is enclosed by erosional walls. In the deflation basin, most erosion and aeolian transport can be found. At the downwind end of the blowout a depositional lobe will form, which is an accumulation of sediment (Hesp, 2002; Hesp & Hyde,

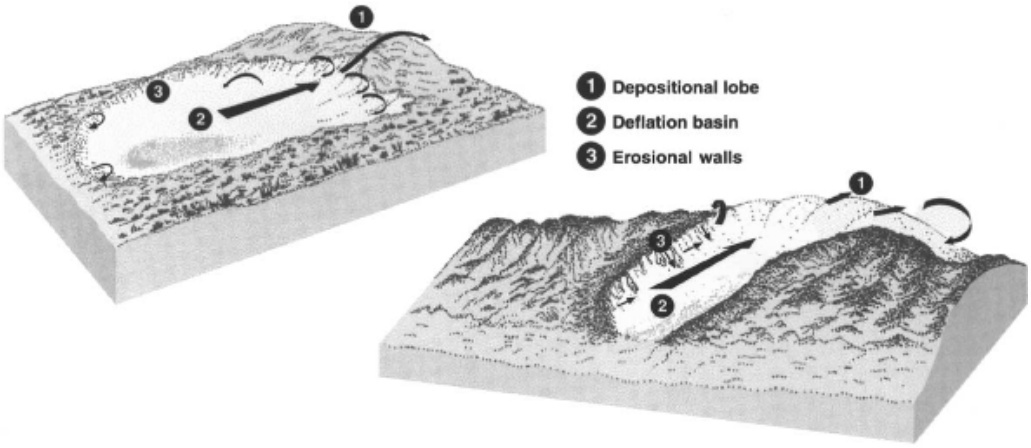

Figure 2.2: *Morphology of the two most common blowouts with the inclusion of the dominant wind and transport direction. Left: saucer blowout, right: trough blowout. Source: Hesp (2002).*

1996). The blowout grows when more sand is eroded in the deflation basin and is transported towards the depositional lobe, back dunes or is transported from the beach inland.

Complex interactions between wind flow, the morphology of the blowout and sediment transport control the morphodynamics of blowouts. Topographical steering will occur as the wind interacts with the surface topography, the magnitude of the wind may change (i.e., acceleration or deceleration) and direction of near-surface flow vectors can alter (Walker et al., 2017). Despite the large degree of spatial and temporal variability in blowout morphologies and aeolian environments, Cooper (1958) classified two primary types of blowouts, saucer- and trough blowouts (Figure 2.2). The saucer blowout is semi-circular or saucer shaped feature with a large width-to-depth ratio. Over time, these can evolve into deeper bowl-shaped (or cup-shaped) blowouts. Trough blowouts are distinguished by a narrow entrance known as a blowout 'throat,' with steep erosional walls enclosing a relatively deep deflation basin (Hesp, 2002; Hesp & Hyde, 1996; Hesp & Pringle, 2001). For the remainder of this thesis, this ‘throat’ will be referred to in a general term as the mouth of the notch. Compared to saucer blowouts, trough blowouts are often more elongated and have a smaller width-to-depth ratio (Hesp & Walker, 2012).

2.2.1 Initiation of blowouts

Blowouts are common in coastal dunes that are occasionally eroded and/or receding. Nonetheless, they can also be found in more stable and accretionary areas with high winds and waves energy, such as coastal dunes along the Dutch and Danish coasts (Arens et al., 2013; Clemmensen et al., 2014). Furthermore, the dune shape, the wind direction and intensity all play a role for the type of blowout that will form (Jungerius et al., 1991). The orientation of blowouts is usually the same as in the predominant wind direction (Hesp, 2002). Saucer blowouts are typically found on foredunes with a broad crest, whereas trough blowouts are more likely on foredunes with a steep, windward facing slope (Hesp & Walker, 2012). In addition to the morphology of the foredune, which is an important factor for blowout initiation, Hesp (2002) listed seven other ways that can initiate the formation of blowouts:

1. Wave erosion: continuous wave action can erode the seaward face of the foredune, which, in combination with wind, can erode the fresh unvegetated parts, causing a breach in the dune. This might be the onset of the formation of a blowout.
2. Topography-related wind erosion: topography can accelerate airflow in various ways but is often the result of irregularities in the dune morphology. Increased wind velocity can cause higher erosional rates, allowing a small depression to grow and eventually form a blowout (Gares & Nordstrom, 1995).
3. Climate change: climate change has affected blowout development in the past and probability will continue to do so in the future. Wind erosion is more likely to result in the formation of blowouts when vegetation is weakened by for example increased storm frequency, prolonged droughts, and/or a drop of the water table. Over longer time periods, wind direction and velocity may alter and change the initiation of blowout formation.
4. Variations in vegetation in space and through time: the density of the vegetation fluctuates throughout both time and space. Areas with less resilient or dense vegetation are more vulnerable to erosion. This can be initiated, for example, by soil nutrient depletion, human induced weakening/ removal of vegetation or when vegetation is grazed by animals.
5. Water erosion: water erosion is not often considered as a mechanism for the formation of a blowout, but it can contribute to it. Surface erosion from sheet wash and raindrop splash can occur during moderate to heavy rainfall, and gullies and rills with associated debris fans can emerge. These disturbances are vulnerable to wind erosion (see condition 2: topography-related wind erosion) (Jungerius & Van der Meulen, 1989).
6. Extreme wind erosion: extreme storms or hurricanes can undercut and bury vegetation, leaving a bare surface which is favorable for the blowout formation.
7. Human impact: finally, human impact on coastal dunes can be enormous. Since humans settled in the coastal region, the landscape has seen several changes. For instance, the dunes were cultivated, damaged by pedestrian trampling and the construction of paths (Bate & Ferguson, 1996), and the vegetation was affected and altered (Arens et al., 2013; Hesp, 2002; Schwarz et al., 2018). Furthermore, in the last decade, a significant number of foredunes have been excavated to artificially generate blowouts (Ruessink et al., 2018).

The second (topography-related wind erosion), fourth (variations in vegetation in space and through time), and seventh (human impact) are particularly important, considering this thesis initiation conditions. Between October 2012 and March 2013, the five notches were excavated in the former 20-m-high established foredune in National Park Zuid-Kennemerland (NPZK) near Bloemendaal, the Netherlands. These foredune notches were excavated to enable transport of beach sand into the back dunes. The landscape transformation would not have occurred without human intervention, and the foredunes would have remained static (Arens et al., 2007).

2.2.2 Dynamic blowout development cycle

Depending on the local morphologic and ecological conditions, a blowout will continue to grow until it reaches its maximum extent. Schwarz et al. (2018) divided the blowout

development cycle into three stages, which they referred to as the bio-geomorphological succession. This describes all stages of a blowout, including blowout initiation and stabilization, and foredune recovery. Figure 2.3 shows the conceptual model of the three phases and the relative influence of abiotic/biotic processes. Interaction between biotic (ecological) and abiotic (environmental) factors reveals the stage of a blowout within the development cycle. Sand movement, wind speed, rainfall, and temperature are examples of abiotic processes. Biotic processes include the pace of vegetation growth, seasonal variation, and competition. Three successional phases were proposed: geomorphologic, bio-geomorphological, and ecological (Schwarz et al., 2018).

During the geomorphological phase, abiotic processes are dominant and can initiate a blowout in established foredunes. Vegetation can be affected by physical disturbances (e.g., floods and storms) and might be damaged and/or removed (Corenblit et al., 2015). This geomorphological phase also includes the seven factors of Hesp (2002) discussed earlier (chapter 2.2.1). The impact of abiotic processes decreases as vegetation begins to re-establish along the sides of the deflation basin and on the depositional lobe. Plants interact with the wind increasing resistance, resulting in increased local sand deposition. The abiotic and biotic processes interact and bio-morphodynamic feedback mechanisms form. When the blowout takes on a distinct shape (e.g., trough, saucer), it will shift to the biomorphological stage. The bio-morphodynamic feedback mechanisms are most effective when the abiotic and biotic processes are in an equilibrium (Schwarz et al., 2018). When no storms occur and reset the blowout, plants can eventually re-colonize the entire blowout. There will been a transition to the ecological phase where vegetation controls environmental development (Corenblit et al., 2015; Schwarz et al., 2018; Van Boxel et al., 1997). Soil development will contribute to the stabilization of the blowout and, eventually, can transform into a parabolic dune during blowout closure (Carter et al., 1990).

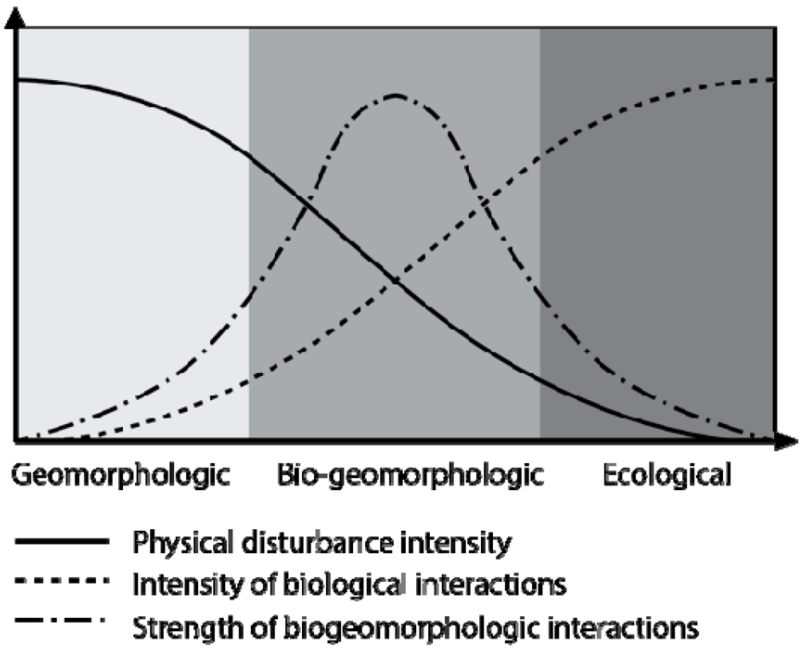

Figure 2.3: the bio-geomorphological succession on blowout development including three phases and intensity of feedbacks between biotic and abiotic processes. Source: Schwarz et al. (2018).

This development cycle occurs on a decadal scale; however, this is affected by the size of the blowout (Gares & Nordstrom, 1995). The blowout may be revived, and the development cycle may be repeated depending on the presence of significant abiotic activities (Barchyn & Hugenholtz, 2013).

Van Kuik et al. (2022), found that the surface areas of blowouts did not only vary on multi-annual (decadal) scale but also on seasonal, and episodic time scales. They described the multi annual scale to reflect successive development, like Schwarz et al., (2018) proposed with the bio-morphological succession. In the winter, larger blowout areas were observed, this seasonal variations in blowout area (seasonal scale) are related to the latitude of the site. The variation reflects seasonal vegetation development and the impact of stronger winds in winter. Episodic increases in blowout area are linked with severe foredune erosion. However, none of the episodic events pushed blowouts into a different stage (multi annual or the bio-geomorphological succession of Schwarz et al., (2018)) or had a long-term impact on seasonal dynamics.

2.3 AEOLIAN SEDIMENT TRANSPORT

The transport that is induced by wind-related forces, is called aeolian sediment transport. Sediment transport through fluid forcing has been extensively investigated, both in laboratories and in the field. Although the concept is quite well understood, the physics behind the aeolian sediment transport is very complex and generally accepted equilibrium theories are only applicable in very rare cases. When wind velocity becomes larger than the threshold, sand can be lifted and transported by saltation (Bauer et al., 2009). The predicted transport rates diverge more from the observed transport rates as the complexity of the sediment transport system increases. The degree of complexity depends for example on inherently complex phenomena (e.g., turbulence), the moisture content and the grain size.

2.3.1 Transport modes

In beach-dune systems, there are four modes of aeolian sediment transport that can develop when the wind shear stress is sufficient enough to lift and move the sediment: suspension,

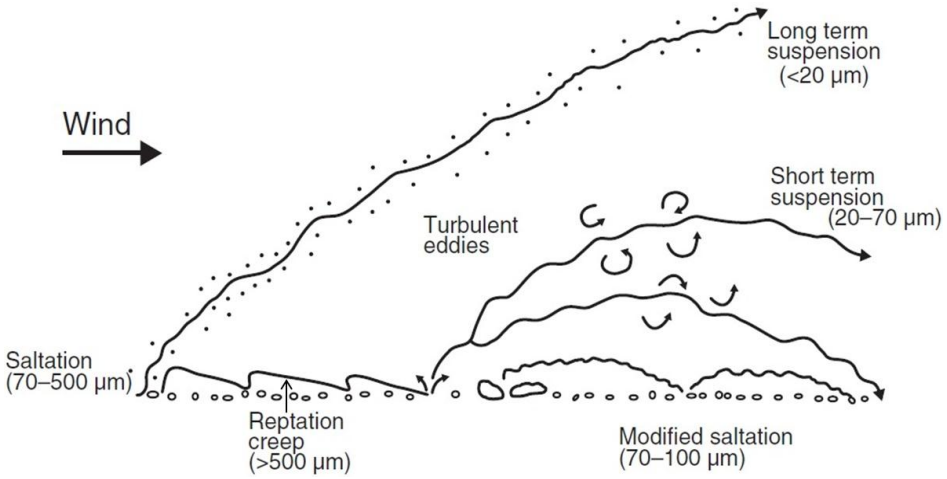

Figure 2.4: schematic of the four modes of sediment transport. Source: Nickling & Neuman (2009)

saltation, creep and reptation. When particles are small enough (<20 um) they can enter a long-term suspension (Gillette et al., 1997, Figure 2.4 long term suspension). Saltation is the dominant mode of transport, which is best described as short-term suspension, and can only take place when the sediment particles fit within the appropriate size range (Figure 2.4: saltation). Larger particles (>500 um) would not be able to enter suspension and are only able to make brief jumps, known as “reptation,” or roll over the surface, known as “creep”. These four modes of transportation are depicted schematically in Figure 2.4. In this thesis, saltation is the primary mode that is examined; the other modes (suspension, reptation, and creep) are not covered in this study.

2.3.2 Fetch effect and moisture effect

The potential amount of sand transport is affected by the length of the fetch and the degree of soil moisture. As saltating particles lose their buoyance and hit the ground, their momentum can be transferred into other particles, these may be detached from the ground and become (short-term) suspended. This effect, known as ‘avalanching’ (Chepil, 1957) or the ‘saltation cascade’ (e.g., Bauer et al., 2009), could theoretically lead to infinite growth of transport. Increases in transport rates tend to increase the aerodynamic roughness of the surface layer (Gillette et al., 1996). This improves the momentum transfer of the airborne particles when hitting the surface and thus transport rates increase even more. This feedback mechanism is known as the 'Owen effect' (Gillette et al., 1997), and, along with the avalanche mechanism, forms the 'fetch effect' (Anthony, 2008). However, every aeolian transport system has a saturation point, at that point the system can simply not transport more sediment (e.g., de Vries et al., 2014). The main factors influencing its capacity are the wind speed, sediment grain size, and moisture content (Bauer & Davidson-Arnott, 2002).

The fetch (F) is determined by beach geometry (W, L) and wind incidence angle (α) (Delgado-Fernandez, 2010) (Figure 2.5). Oblique winds naturally result in longer fetches than cross-shore winds, while the fetch is infinite for perfectly alongshore winds. The total distance from the swash line (i.e., upwind boundary) to the dune line parallel to the wind is the maximum potential fetch (Fm). In contrast, the critical fetch (Fc) is the minimum distance required for the sediment transport system to reach equilibrium (or saturation) and this critical distance can vary depending on e.g., the wind speed (Bauer et al., 2009). Sediment transport rates in

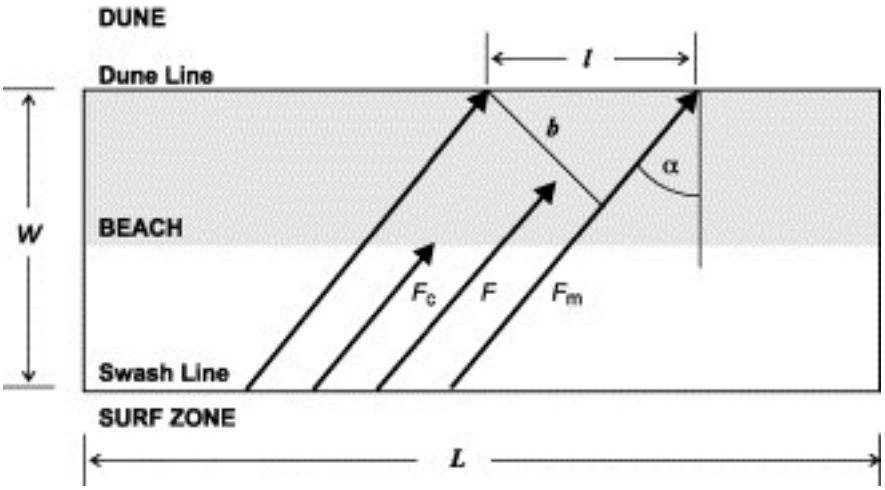

Figure 2.5 *Schematic of beach dune system WxL with fetch terms discussed in text. Source: Bauer & Davidson-Arnott (2003).*

the blowout/excavated notch are dependent on the amount of transport on the beach. A relatively large amount of sand can enter the notch if there is a lot of transport on the beach. Maximum transport rates in the notch are not reached when the fetch (Fm) on the beach is smaller than the critical fetch (Fc), this is especially the case with narrow beaches where for most wind directions the critical fetch cannot be reached. The transport capacity of the wind (at a given wind speed) is finite (Delgado-Fernandez, 2010). When the fetch exceeds the critical fetch, the self-balancing mechanism tend to stabilize the transport rates. However, a change in the surface properties, such as roughness (e.g., during increasing transport rates), moisture content or temperature, causing a modification of airflow downwind of the discontinuity. This may lead to downwind vertical expansion of the internal boundary layer, decreasing the overall shear stress distribution, reducing the wind transport capacity from the beach to the foredune (blowout), and this makes reaching an equilibrium unlikely (Bauer et al., 2009).

Moisture stored in the top layer of the soil can alter the transport rates drastically since it strengthens the cohesive forces between the soil particles (Chepil, 1957). The so-called "moisture effect" typically results in a significant reduction in transport or may even lead to a total shutdown, even when the threshold velocity is raised sufficiently (Arens, 1996; Bauer et al., 2009). When moisture content becomes higher than 10% transport will cease completely, how values below this threshold of moisture content affect the transport rates is still not complete clear. Environmental factors that influence local moisture levels in the soil are precipitation, humidity, and groundwater table (Bauer et al., 2009). The groundwater table is typically significantly below the dune subsurface, making atmospheric humidity and precipitation the most crucial factors for this thesis.

2.3.3 Wind forcing and turbulence

De Vries et al. (2014) discovered that it is more likely that the dependence of sediment transportation on wind speed is linear than as a third-power relationship under supply limited conditions, as it is commonly described. Variations in precipitation intensity, tide level, and wind direction are other factors that influence this dependency (Bauer et al., 2009), as they are related to the mechanisms described in 2.3.1 to 2.3.2. Wind is neither uniform nor steady under natural conditions (Wyngaard, 1992) and turbulence remains a largely unsolved problem in classical physics (Smits and Marusic, 2013). Due to its inherent complexity of the wind, there is also much variability in sediment transport rates (Bauer et al., 1988). Moreover, individual saltating grains retain their momentum even during airflow accelerations or decelerations, resulting in ‘saltation inertia’ (Spies et al., 2000). The response time of the transport to a deceleration in wind velocity is often 1 to 2 seconds, while it is responding almost instantly to accelerations (Butterfield, 1993).

2.3.4 Aeolian sand streamers

The inherent complexity of the wind results in the formation of aeolian streamers. These streamers are highly intermittent, snake-like features that shifts laterally while propagating in a streamwise fashion (Baas & Sherman, 2006; Gares et al., 1996). These complex and dynamic transport patterns of the aeolian-streamer phenomenon fluctuate in both time and space on scales of 0.1 s and 0.1 - 1.0 m (spanwise; wind-normal) (Baas, 2008). Traditional

aeolian saltation transport models do not account for the spatiotemporal variability and generally oversimplify the transport mechanism into a steady and uniform saltation sheet which is a function of the time-averaged wind speed (Baas, 2008). This method often results in significant differences between predicted and observed transport rates (Ellis et al., 2012). The intermittent nature of streamers effectively diminishes the amount of time over which transport occurs (Davidson-Arnott & Bauer, 2009).

Baas (e.g., 2004, 2006, 2008) probably conducted the most extensive research on aeolian streamers, which was elaborated in several subsequent papers. He discovered that over a homogenized surface, bed surface control (e.g., microtopography, moisture content, or grain size) does not play a significant role in the development of streamers. Streamer characteristics may differ from site to site, based on the quantity, distribution, and properties of the erodible material at the surface.

To explain streamer dimensions and behaviour, Baas and Sherman (2005) created contour maps. They distinguished three mutually exclusive saltation transport patterns: streamer families, nested streamers, and clouds with embedded streamers, which occur under low-, intermediate-, and high-intensity transport conditions, respectively. It is challenging to successfully and accurately capture streamers using an Eulerian method because they are constantly varying transport phenomena that intertwine, merge, and split apart at the same time (Sherman et al., 2013). Sherman et al. (2013) discovered the average flow-parallel length scales of streamers are in the 10s of metres, with distance between centres of different streamers ranging from 0.6 to 1 m and leaving gaps between individual streamers of about 0.2 m. Despite the differences in the natural setting, these findings are consistent with those reported by Baas and Sherman (2005).

Baas and Sherman (2006) examined the effect of the aeolian-streamer phenomenon on the spatial variability in saltation intensity. They discovered that average variability in saltation intensity ranged from 29% (for the smallest spanwise and largest temporal scale) to 266% (for the largest spanwise and smallest temporal scale). The variability tends to stabilize beyond approximately 3 m for most time-averaging periods. Ellis et al. (2012) found similar values and suggested that the decline in variability for greater sample duration and transport intensity to capacity of streamers to smooth variability through lateral migration. These results emphasize the potential influence of streamer transport on the inherent error margins of many numerical saltation transport models that are based on extrapolation.

2.4 AEOLIAN SEDIMENT TRANSPORT WITHIN A BLOWOUT

The development of a blowout is the result of interaction between sediment supply and vegetation. It is crucial to understand how the sand is transported to understand how it may affect the morphological development of the blowout. When wind velocity exceeds a certain threshold (Chapter 2.3.1; Bauer et al., 2009), sand is lifted and transported to the stoss side of the foredunes. The wind accelerates over the stoss side of the foredunes, on the lee side flow separation occurs decreasing the velocity of the wind and will be deposited (Hesp & Hyde, 1996).

Most natural blowouts are initiated in areas where the prevailing wind direction is onshore; the type of blowout that will form determined by the morphology of the foredunes (Hesp, 2002; Hesp & Hyde, 1996). When the wind comes predominantly from a fixed direction, the shape of the blowout will be more elongated, whereas when the wind direction is more variable, the shape is less defined (Jungerius et al., 1991). Trough blowouts, the natural equivalent of excavated notches, are distinguished by a narrow entrance known as a blowout 'throat,' with steep erosional walls enclosing a relatively deep deflation basin (Chapter 2.2; Hesp, 2002; Hesp & Hyde, 1996; Hesp & Pringle, 2001). A depositional lobe, which is an accumulation of sediment, can be found at the downwind end of the blowout (Hesp, 2002; Hesp & Hyde, 1996). The complex interactions between wind flow, notch morphology and sand transport control the morphodynamics of excavated foredune notches. Topographical steering will occur as the wind interacts with the surface topography, the magnitude of the wind may change (i.e. acceleration or deceleration) and direction of near-surface flow vectors can alter (Walker et al., 2017). Sand will be transported from the beach and the deflation basin to the depositional lobe and into the back dunes due to the morphology of the blowout (Carter et al., 1990; Hesp, 2002; Hesp & Hyde, 1996).

When the morphology of an excavated notch causes flow deceleration, sand will accumulate inside the notch. Over time, the notch will be entirely filled with sand and the notch requires re-excavation. In contrast, a successful excavated notch will allow flow streamline compression (the wind flow from the wide beach into the narrow notch, it is squeezed together as soon as it enters the notch, which causes the flow lines to converge), flow steering and acceleration from the beach to the notch. High wind speeds through the notch will enhance the amount and distance of sand transport to the backdune. Additionally, the presence of jet flows inside the notch may extend the distance of sediment transport from the beach to the backdune (Nguyen, 2022). The aim is that these notches become part of the natural aeolian dynamics, and thereby becoming a self-maintaining phenomenon. However, experience with their performance is limited (Ruessink et al., 2018), therefore most projects are based on trial and error.

In general wind flow is quite well understood and described, however the wind flow around blowouts (in three-dimensions) has yet to be accurately quantified. This is largely due to lack of sufficient airflow measurement and appropriate airflow models (Smyth et al., 2012). Various quantitative studies have been conducted using smoke bombs that have concluded that temporal and spatial variations in sediment transport occur with the presence of turbulent flow structures (Hesp & Hyde, 1996; Hesp & Walker, 2012). However, because of the nature of anemometric data, the flow structures are difficult to quantify, and remains mostly conceptual (Smyth & Hesp, 2016).

2.4.1 Approach angle of the wind

Smyth and Hesp (2016) used high resolution, three-dimensional computational fluid dynamic modelling to investigate the turbulent flow structures within a trough blowout. They found that the efficiency of a trough blowout as a corridor for wind-blown sediment depends on the direction of the incident wind. When the incident wind flow was parallel to the blowout axis, only minor flow steering occurred, but a well-defined near surface jet emerged along the deflation basin. In contrast, no near surface jet was created when the incident wind flow was oblique to the blowout axis (angle of 45°). However, the wind flow was steered along the

blowout axis. Although wind with oblique angles may be steered along the axis of blowout, the relative effectiveness of eroding and transporting sediment appears to be substantially lower when compared to parallel wind flow at the same incident wind speed. Corkscrew or helicoidal vortices were not observed in either incident wind direction.

Nguyen (2022) found that flow streamline compression, wind realignment and acceleration only occur when the angle between the incident wind and the notch axis is 27° or less. When the angle is more than 27°, flow separation and deceleration occur. This contrasts with Pease and Gares (2013), who found that for approach angles within 50° of the blowout axis, topographic steering and realignment of the wind occurs. As the approach angles become more oblique and approaches the 50° of the blowout axis, the wind flow is forced to ever greater amounts of realignment and therefore the amount of steering increases. When approach angle of the incident wind exceeds 50 degrees, wind is no longer steered into the trough mouth in considerable numbers, but instead flows perpendicular to the axis across and over the blowout. Secondary flow in the blowout trough becomes increasingly dominant under those conditions. When wind is steered into and accelerated through the blowout (angle smaller than 50°), it increases transport potential. Angles greater than 50°, on the other hand, result in the blowout trough having little transport potential because secondary flow reduces the net wind speed in the trough and disrupts the flow direction (Pease & Gares, 2013).

2.4.2 Secondary air-flow structures and sediment transport in a blowout

Sediment transport within blowouts has been studied in a variety of ways, only but three studies looked at sediment transport in relation to wind velocity. Two of these were conducted over long periods of time, ranging from days (Hesp & Hyde, 1996) to months (Pluis, 1992). In addition to researching the relationship with wind speed on a much smaller time scale (25 Hz), Smyth et al. (2014) also studied the link between secondary air-flow structures and sediment transport in a trough blowout. This was very useful since zones of streamline compression, expansion, and steering are not as clearly defined in blowouts as in other parts of the dune system (e.g., the stoss slopes and lee of sand dunes)(Smyth et al., 2014). The locations of zones with secondary air-flow structures remain relatively constant at different wind speeds (Smyth et al., 2011, 2013), but changed much for different approach angles of the wind (Hesp & Pringle, 2001; Pease & Gares, 2013).

Smyth et al. (2014) took measurements at five different locations within the blowout: three different locations in the deflation basin, one in the throat and one on the depositional lobe. The wind flow was measured using six, three-dimensional (3D) ultrasonic anemometers and the sediment flux was monitored using eight sand traps. Wind speed and Turbulent Kinetic Energy (TKE) were calculated for various averaging intervals (10 seconds and 1 minute). Turbulence is defined as the deviation of airflow from the mean, large quantities of turbulence may thus have a significant impact on sediment transport. The correlation between sediment flux and wind parameter became more apparent as the averaging interval was raised from 10 seconds to 1 minute. They discovered a negative relationship between coefficient of variation (CVk) of the wind speed and sediment flux, indicating that as wind flow variability increases, sediment flux decreases. Because of this, the erosional wall crest, where

flow was compressed and accelerated, recorded the highest rates of sediment transport. In contrast, the deflation basin, which experienced topographic flow steering and deflection during the oblique incident wind, recorded the lowest flux rates. The correlations (between sediment flux and wind parameters) were strongest in the centre of the blowout and weakest close to the erosional walls (Smyth et al., 2014). Wind speed correlated best with sediment flux at 10-second intervals. At minute scale averaging intervals, however, they discovered that TKE may be a stronger predictor of sediment transport than wind speed and therefore may be a better predictor of sediment flux (Smyth et al., 2014).

2.5 RESEARCH QUESTIONS

"As stater previously in this study, long-term the bio-geomorphological succession and dynamics of blowouts are quite well understood. These long-term changes are caused by a series of wind events, each of which contains complex wind phenomena with a high degree of turbulence. These unique wind phenomena, as well as their relationship to sediment transport, are not fully understood. In addition, the best method to excavate foredunes notches is not yet known and is largely based on trial and error. The dune management can be improved by learning more about the processes within excavated notches and blowouts. Although Smyth et al. (2014) found valuable results concerning the relation between wind (e.g., wind speed, CVk and TKE) and sediment transport in a blowout, further research can be done on this topic. For example, the data output of that study was limited, the measurements were primarily conducted in the back of the blowout (deflation basin and depositional lobe), and the measurements have only been performed under limited wind conditions. Furthermore, it can be examined whether data processing can be advanced by, for example, looking at if different temporal averaging intervals would give a stronger correlation (instead of 10 seconds and 1 minute, for example 5-, 10- or 30 minutes intervals). In addition, since most studies mainly looked at the processes in the middle and back of blowouts/excavated notches (e.g. Smyth et al., 2014; Smyth & Hesp, 2016), it is very useful to study the transition from beach to the notches (the notch mouth). Therefore, there are numerous opportunities to conduct new research on this topic. The main research goal and associated sub-questions are:

The main goal is to improve understanding of aeolian sediment transport rates in the mouth of a foredune notch

1) What is the correlation (relation) between sediment transport and different wind characteristics such as wind speed and Turbulent Kinetic Energy?
    a. How does the relation change for different temporal averaging intervals? (What is the best temporal averaging interval?)
    b. What is the relation between sediment transport and different wind characteristics (Wind speed, TKE)?
    c. What is the relation between coefficient of variation of the wind (CVk) and sediment transport rates? And the coefficient of variation of the sediment transport (CV)?
2) What is the spatial variation of sediment flux in the notch mouth as a function of wind approach angle?

3. METHODS

Field experiments were conducted during a field work from 10 October to 4 November 2022 in an excavated notch in the National Park Zuid-Kennemerland (NPZK) near Bloemendaal, the Netherlands (between regional beach poles with km-indication 59,25 and 60,25). This was part of a larger field campaign known as AEOLEX-III (a combination of 'aeolian' and 'experiment'). The aim of the fieldwork was to collect data on the local wind and wind-driven sand transport. This data was collected in the second notch from the south (N2, Figure 3.1) which is one of the five excavated notches.

3.1 SITE DESCRIPTION

Prior to the excavation of the five notches, a 20-m high continuous established foredune existed in the study area NPZK (Ruessink et al., 2018). Due to decades of management, this foredune was completely covered with European marram grass and the dune experienced minimal sand loss (e.g., Klijn, 1981). The management, which included planting marram grass and constructing sand fences, ensured that the foredune became a straight sand 'dike'. These measures ended in 1984, the foredune became more natural, allowing the formation of e.g., embryo dunes (Arens, 1999). In recent decades, the sand budget in NPZK has been slightly positive (Luijendijk et al., 2011).

Various measures were taken in NPZK in 2012 and 2013 to restore dune mobility and thereby increasing the area of the Nature 2000 white dunes habitat while also improving conditions

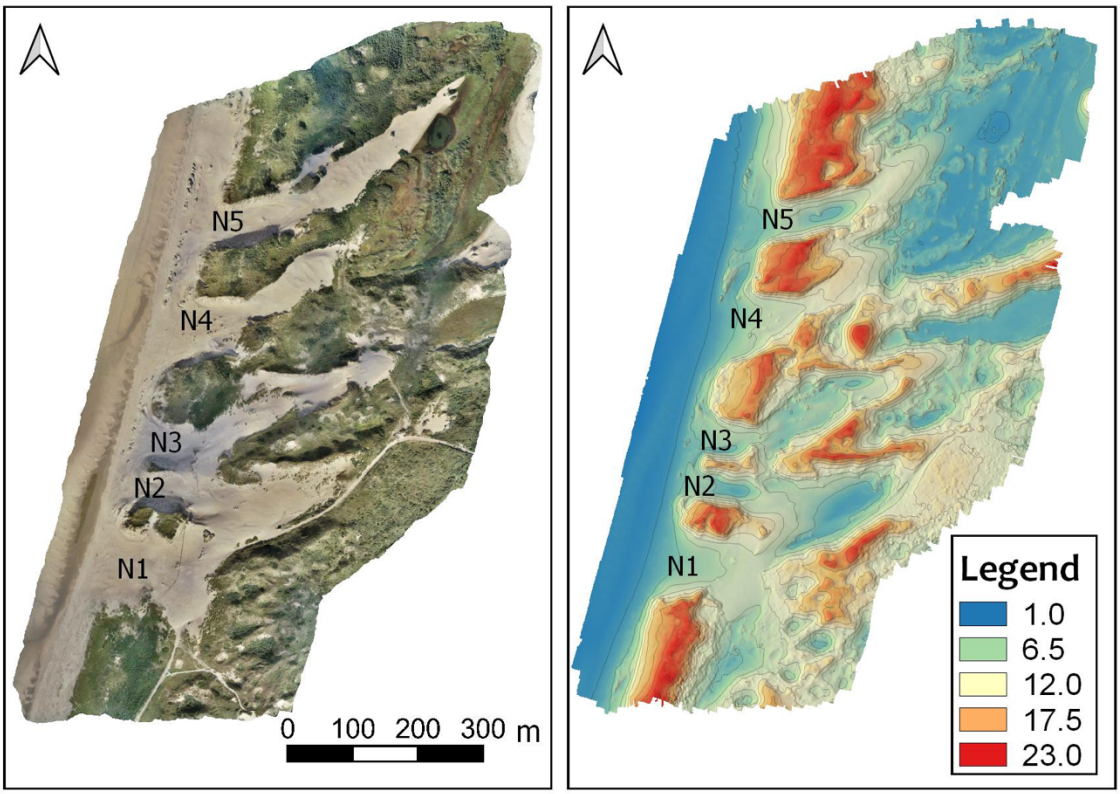

Figure 3.1 Overview of fieldwork area captured on 10/10/2022, with five notches indicated with N1-N5. Left: aerial photo, right: DEM. Data used extracted from DOI 10.5281/zenodo.7010095

in the grey dunes. The measures were all part of the '*Noordwest Natuurkern'* project (Kuipers et al., 2016), and they were divided into two parts: reactivating of existing parabolic dunes and excavating foredune notches. Between October 2012 and March 2013, the five notches were excavated between (beach) km-poles 59.25 and 60.25 (Figure 3.1, labeled N1 to N5 from south to north).

The notches are made in such a way that they extent all the way through the foredune, in an approximately linear slope from about 6 m above Mean Sea Level (MSL) on the seaward side to approximately 9 m on the landward side. N2 had a cross-dune length of 100 m, a width of about 50 m and had a V-shape at the start. The orientation of N1-N3 is about shore normal, while N4 and N5 have a slightly more southwest-northeast orientation. There only have been few interventions since the excavation in 2013. In 2013 and 2014, marram grass was removed in the notches at seaward side of the notches, additionally a gravel path was removed. Occasionally remnants from World War II Atlantic Wall bunkers are removed when they become exposed due to erosion. The public cannot access the notches, excluding N1, which also serves as a beach entrance (Ruessink et al., 2018).

3.1.1 Morphology

In the first three years following the excavation, the notches evolved into a U-shape due to wall erosion, and depositional lobes of 8 meters thick and 150 meters long developed. The sand budget of the entire study area remained approximately the same compared to the pre-notch situation (22,750 m^3 per year). Prior to the notch exaction, all wind-blown beach sand was deposited on the seaward side of the foredune; however, since 2013, 75% of the sand has deposited on the landward side of the foredune. This demonstrates that notches are effective in enabling aeolian sediment transport from the beach into back dunes (Ruessink et al., 2018). Figure 3.2, shows the N2 more clearly with a close-up of the aerial image and DEM captured on the first day of fieldwork.

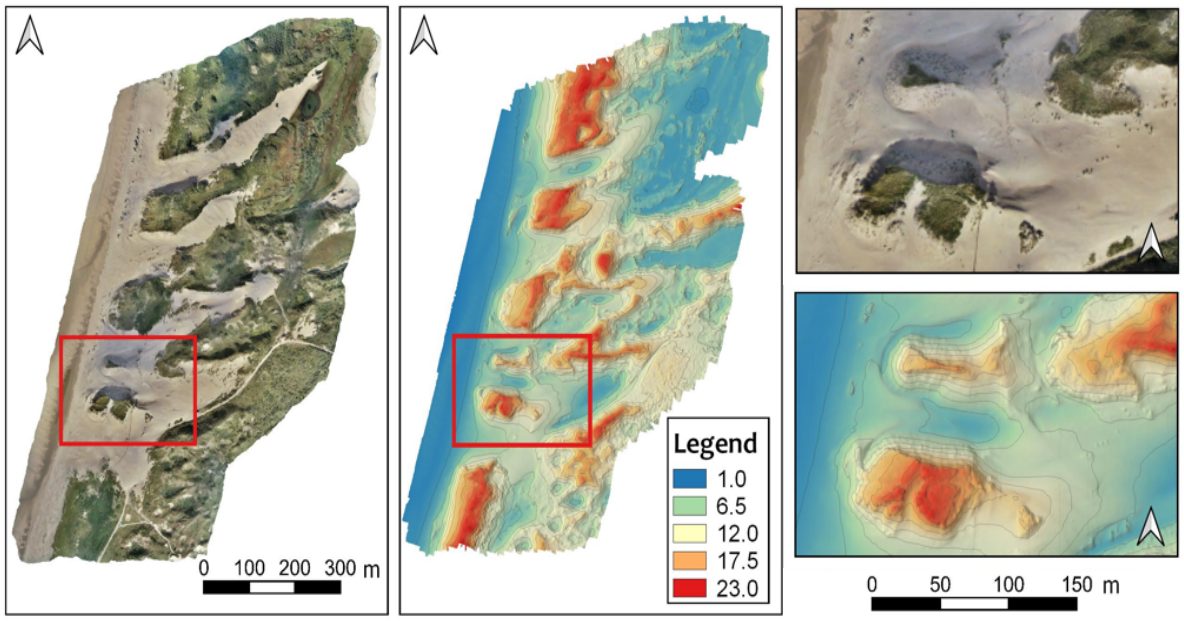

FIGURE 3.2: Overview of fieldwork area captured on 10/10/2022, with close up of N2. Left: aerial photo, right: DEM. The numbers in the legend are in m MSL. Data used extracted from DOI 10.5281/zenodo.7010095

3.1.2 Wind and wave climate

The first wind rose (Figure 3.3, left) depicts regional wind conditions over approximately 15 years preceding and during the fieldwork period (i.e., 2008-2022) measured at station 225 (IJmuiden) of the Royal Netherlands Meteorological Institute KNMI, located about 4 km north of the study site. The other wind rose (Figure 3.3, right) indicates the regional wind conditions during the field work (i.e., 10/10/2022- 4/11/2022). The strongest and most frequent winds are from the southwest. These winds are strongly onshore shore oblique (the shore-normal direction is approximately 287N). Windspeeds of more than 10 m/s also originate from the west to the northwest direction, but these are less prevalent. However, north-westerly winds are frequently associated with a storm surge exceeding 1 m, which, when combined with great waves height (> 5 m), can result in destruction of the embryo dunes and foredune scarping (e.g., De Winter et al., 2015). During the fieldwork, the wind came primarily from the southwest, south, and southeast. As a result, measurements were only taken under those wind conditions.

3.2 INSTRUMENTS

During the entire field campaign a wide variety of instruments was deployed, of which only those relevant to this study are mentioned below. The main tools used in this investigation included those that could simultaneously measure the saltation intensities and wind parameters. A series of additional instruments were deployed in order to collect footage of sand transport on the beach and determine various boundary conditions.

3.2.1 Saltation detection system

Saltation impact sensors were chosen to measure saltation intensity since it requires measuring equipment capable of measuring at a high frequency, to get a thorough understanding of the characteristics of aeolian sand transport in the notch which cannot be achieved with sand traps. The Saltation Detection System (henceforth referred to as SalDec)

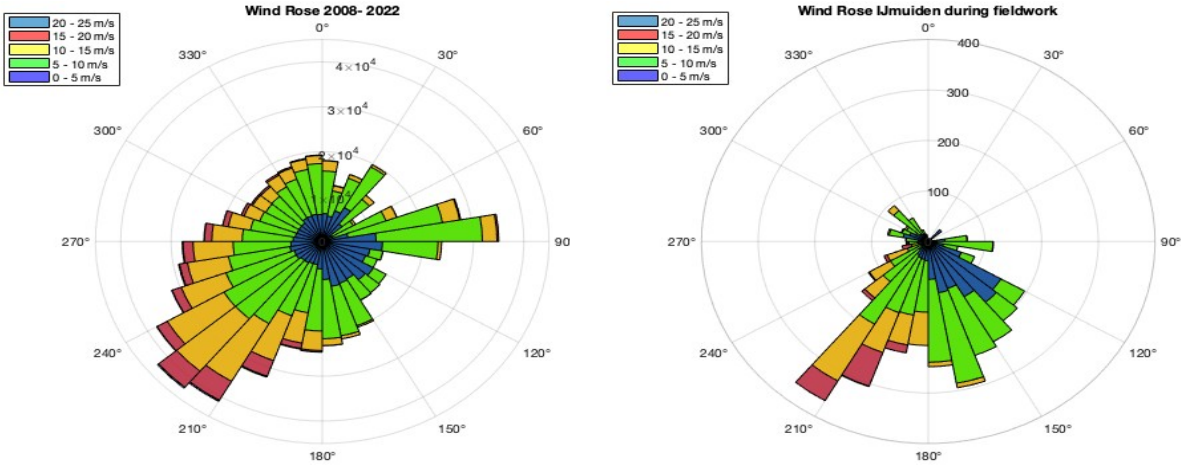

Figure 3.3: Wind roses of wind in IJmuiden. Left: from 2006 till the end of the fieldwork in 2022, right: during fieldwork 10/10/2022-04/11/2022. Data used downloaded from: https://projects.knmi.nl.

was selected since it performed well on most of the desired qualities. A few examples of these qualities are that it has a linear response to changing saltation intensities, the momentum threshold is low enough to detect low saltation rates (but ignores noise from wind gusts, raindrops, or insects) and it must be a low-cost solution. The SalDec is a recently developed instrument, has been tested thoroughly in the lab and performed well (Winter et al., 2018).

During the fieldwork, three identical SalDec's were used to measure the saltation intensity (SalDec02, SalDec03 and SalDec04; SalDec 1 was out of order). Each SalDec was consisting of two rectangular metal bars attached at an angle to one another (Figure 3.4: right instrument). Both horizontal and vertical bars contain eight impact sensors, with the horizontal a spatial resolution of 0.10 m in wind-normal direction over a total width of 0.8 m, while the vertical sensors were placed following a somewhat logarithmic pattern. The lowest sensor connected to the vertical bar had a set height of 0.035 m (midpoint of the sensor) from the bed, the other sensors had heights of 0.90, 0.155, 0.210, 0.275, 0.340, 0.585, and 0.725 m (Figure 3.4: SalDec vertical array). Each sensitive sensor head of the horizontal array, which was spanned in wind-normal direction, was set at 0.10 meters above the bed (Figure 3.4: SalDec horizontal array). Due to accumulation of sand underneath, this might not have remained true during the entire measurement time.

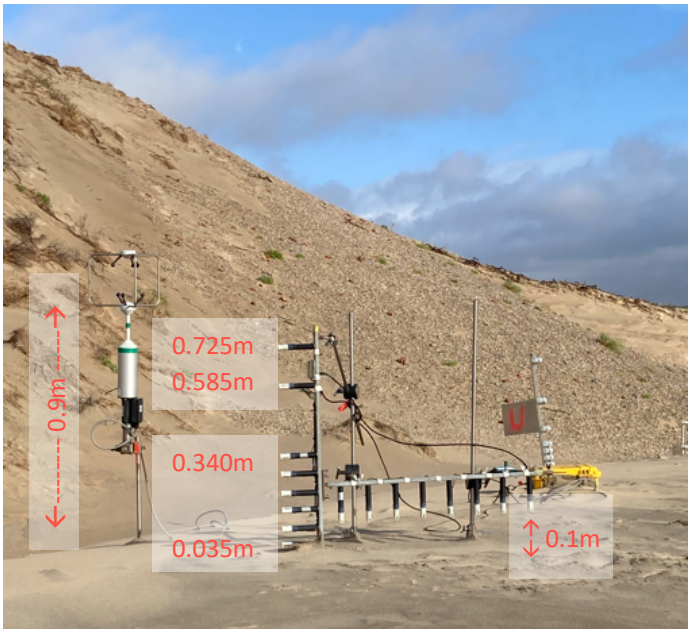

Figure 3.4 Photo of saltation detection system and sonic anemometer set-up in the field

Sensitive piezoelectric elements are mounted in sensor heads with a cylindrical shape, a height of 0.034 m, a diameter of 0.020 m, and a frontal sensing area of about 10.7 cm^2 (Figure 3.4: SalDec white caps) (De Winter et al., 2018). Each sensor provided an analogue voltage signal that was updated with a frequency of 10 Hz based on the number of grain impacts observed (i.e., at a rate). The horizontal and vertical arrays were connected to two separate series that were both connected a counter box, which transferred the signal bundle to a data logger. Thus, one fully operational SalDec provided a total of 16x10-Hz time series of saltation intensity in unit counts/0.1s. De Winter et al. (2018) provide a more detailed description of the SalDec and how it operates electronically.

Although data gained with the SalDec does not provide a direct translation to absolute transport values, it is a consistent measure to determine the relative saltation intensity. At low transport rates, the maximum measured variance in sensitivity to grain impact is 9%, indicated in wind tunnel experiments, but deemed approximately equal in the field (de Winter et al., 2018).

3.2.2 Ultrasonic anemometer

Sonic anemometers (SA, Young Model 81000RE) were used to monitor airflow characteristics, providing three orthogonal components (u, v, and w, accuracy: ±0.1 % rms ±0.05 m/s) of wind and sonic temperature (accuracy: ±2 C) at a frequency of 10 Hz determined using the transit times of ultrasonic acoustic impulses between the sensor heads (Van Boxel et al., 2004).
During the fieldwork, three identical SA (Figure 3.4: left instrument) (Red:SA02, Blue:SA03, and Green: SA04) were deployed, each paired with a SalDecs (with the same number label).

The SA/SalDec set-up formed the most important instrument set-up in this study. It is relatively easy to synchronize and correlate the data taken by the two devices because these operate at the same high sampling frequency. The SA was placed next to the SalDec at a height of 0.90m, but not too close that it may interfere the saltation process at the SalDec (approximately 0.5 m, see Figure 3.4). The location of the SalDec and the SA were selected in such a way that the conditions at both locations were as close as possible. The SA was adjusted to the north using GPS to meet its inner coordinate system, and a bubble level was placed on the SA to ensure that the plane was perfectly horizontal.

Figure 3.5: Set-up of the three SalDecs and sonic anemometers as they were positioned most days. Photo was taken on day 5.

3.2.3 Additional instruments

In the second notch, N2, there are also four fixed sonic anemometers that constantly measure the wind (Figure 3.6: SA02, SA03, SA01 and SA04). The data from SA02, positioned in mouth of the notch, is mainly used in this research. The complex 3D topography of the excavated notch was obtained from highly overlapping images collected with an Unmanned Aerial Vehicle (UAV, e. g., see Ruessink et al. (2018) for workflow) and DGPS, this was done at the start and end of the fieldwork (12 Oct 2022 and 01 Nov 2022). The DGPS is also used to measure the coordinates of all instrument deployments and measurement locations.

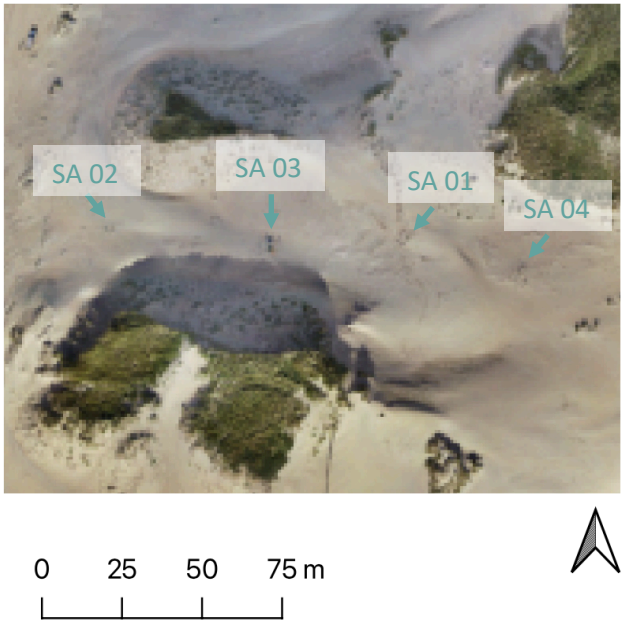

Figure 3.6: Locations of the four fixed sonic anemometers

Figure 3.7 Position of northern SalDec and Sonic Anemometer. Left: on the hills next to the gully on day 5, right: in the northern gully on day 7.

3.3 DATA COLLECTION

3.3.1 Saltation and wind data

Sediment transport and wind data were collected using the three SalDecs/Sonic Anemometer system (hereafter referred to as SSA) on nine days giving nine measurement runs of varying duration, at different locations, and under varying weather conditions. The coordinates of the setup were determined at the location of Sonic Anemometer using an DGPS device. Since the wind was rarely sufficient to transport sand, there were only 9 measurement days in total during the fieldwork period. The first two measurement days were more 'test days' than measuring transport because then there was little or no transport on those days.

The SSAs were positioned at three different locations within the notch mouth perpendicular to the notch orientation/axis, one in the middle and the other two as close as possible to the erosional walls on both sides (Figure 3.5 and 3.8). The location of the three SSAs was determined and is illustrated in Figure 3.8. On the north side, there is a small gully; on some

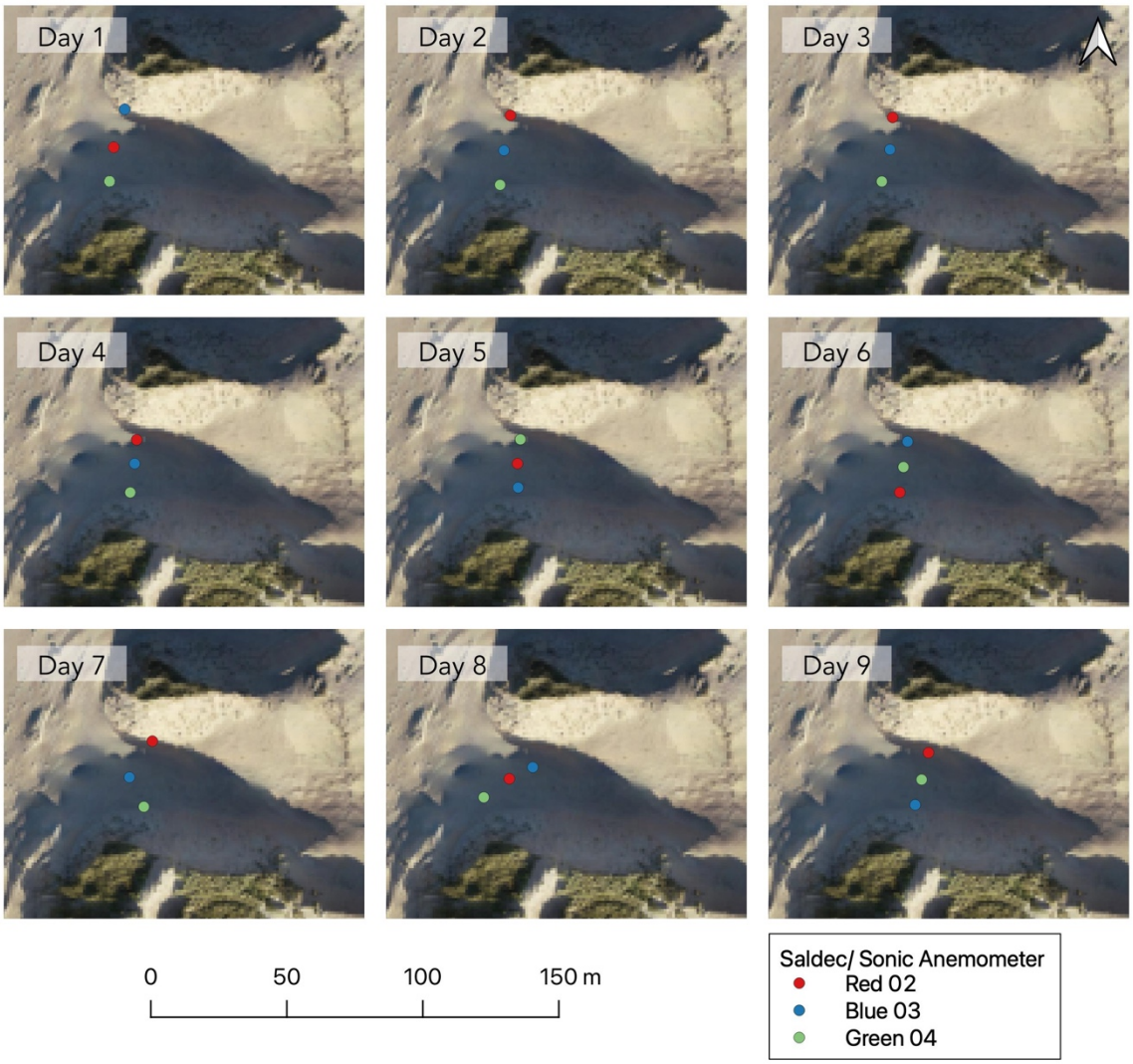

Figure 3.8: Positions of the SalDec and Sonic Anemometers on each measurement day

days, the SSA was positioned slightly south of the gully on the little hill (days 4, 5 and 6), while on other days (day 1, 2, 3, 7 and 9), the SSA was placed in the gully (Figure 3.7). On day 8, the positioning of the SSA was different, and the SSA were placed in such a way that these were in line with the incoming wind.

To prevent confusion, the SSA will only be referred to by its position and not the name of the SSA in the remaining of this thesis (as shown in Figure 3.9).

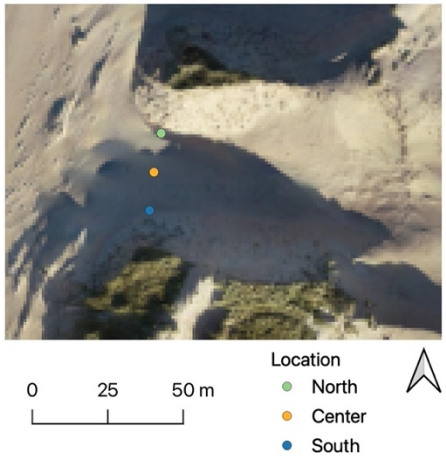

Figure 3.9: This map provides an overview of the position of the SSA that will be referred to in the remainder of this Thesis.

3.4 DATA PREPARATION

The measurements were conducted under sometimes harsh transport conditions, which could lead to complications in the measured data. Data cleaning ensured a data set with significant quality that could be used during analyses. This was accomplished with the help of several scripts created by Bosma (2020), who had made the scripts in MATLAB for data cleaning during his thesis.

3.4.1 Counter box malfunctioning

For the 8 horizontal and/or 8 vertical sensors, it occasionally occurred that minus ones were shown as output instead of a normal value (zero or bigger than zero); the following time step had typically outliers that were roughly twice as large as the previous timestep (Figure 3.10). This error only occurred during periods of high transport intensities, indicating that the counter box got saturated with electronic signals that needed to be processed. Assuming that counts from the timestep with minus ones were added to the subsequent timestep, this was solved by replacing the eight minus ones and the outliers with half the value of that outlier timestep.

3	2	6	9	17	19	11	6	6	0	1	1	2	0	6	5
5	19	10	23	24	21	22	22	9	4	3	2	6	4	5	9
17	28	14	15	21	18	15	22	23	10	13	11	14	13	3	0
23	18	19	17	20	19	24	18	30	14	16	11	7	9	1	1
17	18	22	15	16	15	20	11	21	27	12	5	1	2	3	3
-1	-1	-1	-1	-1	-1	-1	-1	21	16	8	1	1	2	1	5
39	23	43	38	40	31	36	29	-1	-1	-1	-1	-1	-1	-1	-1
14	5	3	3	4	2	2	1	37	39	44	36	12	3	1	0
25	20	8	4	3	6	8	3	11	25	12	7	0	0	1	2
13	20	5	10	6	7	10	11	25	20	9	5	3	4	3	2
25	13	19	25	17	11	25	23	15	21	12	13	6	2	4	8
14	5	14	14	19	25	18	23	0	10	21	16	13	9	5	5
14	13	18	19	16	10	20	20	9	14	12	14	6	5	2	6

Figure 3.10: Example of counter box malfunctioning

3.4.2 Impact sensor saturation

The last step of the quality control determined whether the impact sensors of the horizontal array (measured at 0.1 m above the ground) had potentially experienced saturation

symptoms, if this was not already resolved by the measures outlined above. This was done using the method and scripts of Bosma (2020). The measurements could not be considered accurate under saturated conditions; to determine whether those conditions occurred the vertical sensor array of the SalDec was used. The whole horizontal and vertical array at a timestep was labelled unreliable and removed from the data set if it had at least one of the following conditions:

- The Sonic Anemometer (SA) record displays an error code (both wind and saltation data are needed for correlation)
- $I > 400$ cnts/s
- $I_{V2} = NaN$
- $I_{V3} - I_{V2} \geq 50$ cnts/s
- $I_{V2} < I_{V4}, I_{V5} \ldots I_{V8}$

IV1 represents the saltation intensity measured at the sensor with the lowest position of the vertical array, whereas IV8 was measures at the highest position. Sensor V2 (0.09 m) was used as a reference instead of sensor V1 (0.035 m), because sensor V2 measured at a more similar height to the horizontal array (0.1 m) than sensor V1 which was much closer to the surface.

The second criterion is set to exclude all data when an intensity is higher than 400 counts/s, because accuracy of a measurement deteriorates rapidly beyond this point (see the results of in De Winter et al. (2018), Fig. 11). The last two conditions are used because it is assumed that saltation intensity will be larger at the bottom and decrease with the vertical distance. If this is not the case, either the lower sensors are clogged with sand, or have reached saturation. For the fourth condition, an arbitrary threshold of 50 counts per second was added to avoid data from being marked incorrect, when only a few counts less were recorded by the lower sensor (this can certainly occur at low values and does not mean that the data is incorrect).

3.5 DATA PROCESSING

3.5.1 Saltation intensity

Spanwise mean saltation intensity

At first, the average of the horizontal array is calculated for each time step, since the average saltation intensity is most important for this thesis, while minor spatial fluctuations in saltation intensity (expressed e.g., in streamers, see chapter 2.3.4) will not be investigated.

Equation 1:

$$\mu_y = \frac{1}{8} \sum_{p=1}^{8} I_p = \frac{I_{p=1} + I_{p=2} + \cdots + I_{p=8}}{8}$$

Where μ_y is the instantaneous spanwise mean saltation intensity calculated over the horizontal sensor array for each time step. The instantaneous saltation intensity measured at a specific sensor is indicated by I_p, where the sensor closest to the vertical sensor array is indicated by p=1.

Temporal mean saltation intensity

The following method was used to calculate temporal means from the saltation intensity data. These means were used to improve correlation and identify the best temporal averaging interval for wind parameters and saltation intensity:

Equation 2:
$$\bar{\mu} = \frac{1}{N}\sum_{t=1}^{N}\mu_y(t) = \frac{\mu_{y\,t=1} + \mu_{y\,t=2} + \cdots + \mu_{y\,t=N}}{N}$$

The temporal mean saltation intensity, μ, is calculated over a specified time interval, where *N* the number of observations within that time interval and the instantaneous spanwise mean saltation intensity at timestep '*t*' is indicated with $\mu_{y\,t}$. In addition to the instantaneous scale (i.e., 0.1 s), the following temporal scales were considered in this thesis:

- 1 second (*N*=10)
- 10 seconds (*N*=100)
- 1 minute (*N*=600)
- 5 minutes (*N*= 3000)
- 10 minutes (*N*=6000)
- 30 minutes (*N*=18000)

All the subsequent equation will be calculated for the same temporal averaging intervals.

Coefficient of variation of saltation intensity

The calculation of temporal standard deviation of saltation intensity (σ) can be used as a measure for fluctuations in saltation intensity. To standardize the standard deviation of saltation intensity with respect to the mean of each time interval, the coefficient of variation (CV, or relative standard deviation) of saltation intensity was calculated (Lynch et al., 2013):

Equation 3:
$$\sigma = \sqrt{\frac{\sum_{t=1}^{N}(\mu_y(t)-\mu)^2}{N-1}}$$

Equation 4:
$$CV = \frac{\sigma}{\bar{\mu}} \cdot 100\%$$

3.5.2 Wind data

Wind speed and direction

As the Sonic Anemometers were aligned to the geographical north in the field the *u*, *v* components are positive with wind from the west and south respectively, and *w* is the vertical component positive in upward direction perpendicular to the surface. Total wind speed was calculated by combining the three wind elements (u, v, w) detected by the SA at a sampling rate of 10 Hz. This was calculated for the instantaneous wind speed and for the different temporal averaging intervals (mentioned at Equation 2):

Equation 5:

$$U = \sqrt{u^2 + v^2 + w^2}$$

$$\bar{U} = \sqrt{u^2 + v^2 + w^2}$$

Thereafter, direction was calculated using horizontal flow vectors (u, v) and the arctangent function (ATAN2):

Equation 6:

$$direction = atan2\,(\bar{u}, \bar{v}) \cdot \frac{180}{\pi}$$

Turbulent kinetic energy

Large quantities of turbulence may have a significant impact on sediment transport. Since turbulence is not accounted for by mean wind speed, turbulent kinetic energy (TKE) was estimated:

Equation 7:

$$TKE = \frac{1}{2}\,((\,SD_u^2\,) + (\,SD_v^2\,) + (\,SD_w^2\,))$$

Where turbulence is defined as the deviation of airflow from the mean. In recent field research TKE was applied as an indicator of wind flow fluctuation and turbulence intensities (e.g., Chapman et al., 2012). The standard deviation (SD) indicates how much the instantaneous wind vector (u, v and w) deviates from the mean of that wind vector (ū, $\bar{v}$ and $\bar{w}$) for a temporal interval.

The coefficient of variation of the wind speed

In addition to coefficient of variation of the saltation intensity (CV, equation 4), the coefficient of variation of (or turbulence intensity relative to) the wind speed has been computed, which is defined as:

Equation 8:

$$CV_k = \frac{\sqrt{TKE}}{\bar{U}} \cdot 100\%$$

Where Ū is the mean wind speed (Equation 5) and CVk is the coefficient of variation of the wind speed.

4. RESULTS

4.1 MEASUREMENT DAYS

As discussed in chapter 3.3, measurements were taken on 9 days throughout the fieldwork. The measurement days are depicted in Figure 4.1 with the wind speed and direction at IJmuiden and at the fixed anemometer (SA02) in the mouth of the notch. The black lines represent the notch's orientation (100N and 280 N), while the orange line show the orientation perpendicular to the orientation of the notch (190N). The duration of the measurements differed (Figure 4.1, width of the measurement block is different), but on average the duration was about two hours. The table 4.1 shows the average wind direction and speed during the measurement days for IJmuiden, the fixed anemometer, and the three sonic anemometers that were positioned in the field (with the location of north, center and south). In addition, the total amount of precipitation on that day is listed here.

During the first two measurement days, no sediment transport was usually observed, there was quite a bit of precipitation and there were no severe winds (Table 4.1: approach wind speed (IJmuiden) was only 4 m/s, the values in the notch were even lower). Moreover, there were also some technical issues that caused no measurements to be saved on day 2. Therefore, the first two days were used as 'test' days.

On day 3, 6, 7 and 8, small amounts of transport quantities were seen in the field, with the wind occasionally was sufficient the form some individual streamers, this shows the onset of sediment transport. There was more transport seen on days 7 and 8 than on day 6, while the wind speeds were slightly higher on day 6 (Table 4.1: wind speed higher day 6 at IJmuiden and at fixed sonic anemometer (SA02)). This is most likely due to the rain in the morning of day 6, the sand was still wet (also documented in field notes) and making it more difficult to be transported by the wind. It may be possible that the approach angle of the wind also

Table 4.1: Overview averaged wind speed and wind direction in IJmuiden and at the fixed anemometer in the notch mouth and of the three SSA during the measurement period on the nine measurement days. The last column shows the precipitation on that day.

	IJmuiden		SA mouth		North		Center		South		Total precip
	Dir	Ū	Dir	Ū	Dir	Ū	Dir	Ū	Dir	Ū	
Day 1	165.9	4.35	86.5	2.58	114.7	3.45	80.5	3.38	76.5	2.89	0.0
Day 2	178.5	4.56	165.9	1.89	NaN	NaN	NaN	NaN	NaN	NaN	2.5
Day 3	198.2	7.59	179.4	3.01	169.1	2.48	177.1	3.26	188.5	2.84	2.9
Day 4	240.4	11.04	255.3	7.42	NaN	NaN	261.2	7.16	NaN	NaN	0.4
Day 5	217.5	15.21	240.2	7.74	232.9	5.52	249.9	4.93	269.8	6.48	0.9
Day 6	220.2	9.88	243.2	4.88	238.7	3.45	257.4	3.48	277.9	4.25	0.5
Day 7	200.6	9.61	228.9	3.09	250.6	1.06	240.4	2.66	278.9	4.08	0.0
Day 8	205.6	9.81	238.4	3.61	243.7	3.22	247.3	2.62	246.0	2.77	0.0
Day 9	205.6	16.78	231.5	4.87	253.2	3.51	260.2	6.11	288.0	6.94	4.1

contributed, given it was about 200-205N degrees on days 7 and 8 and around 220N degrees on day 6 (Table 4.1: wind direction 'Dir' at IJmuiden day 6, 7 and 8). The orientation of the notch is approximately 280N degrees, making the wind on day 7 and 8 more strongly oblique (almost perpendicular) in relation to the notch orientation.

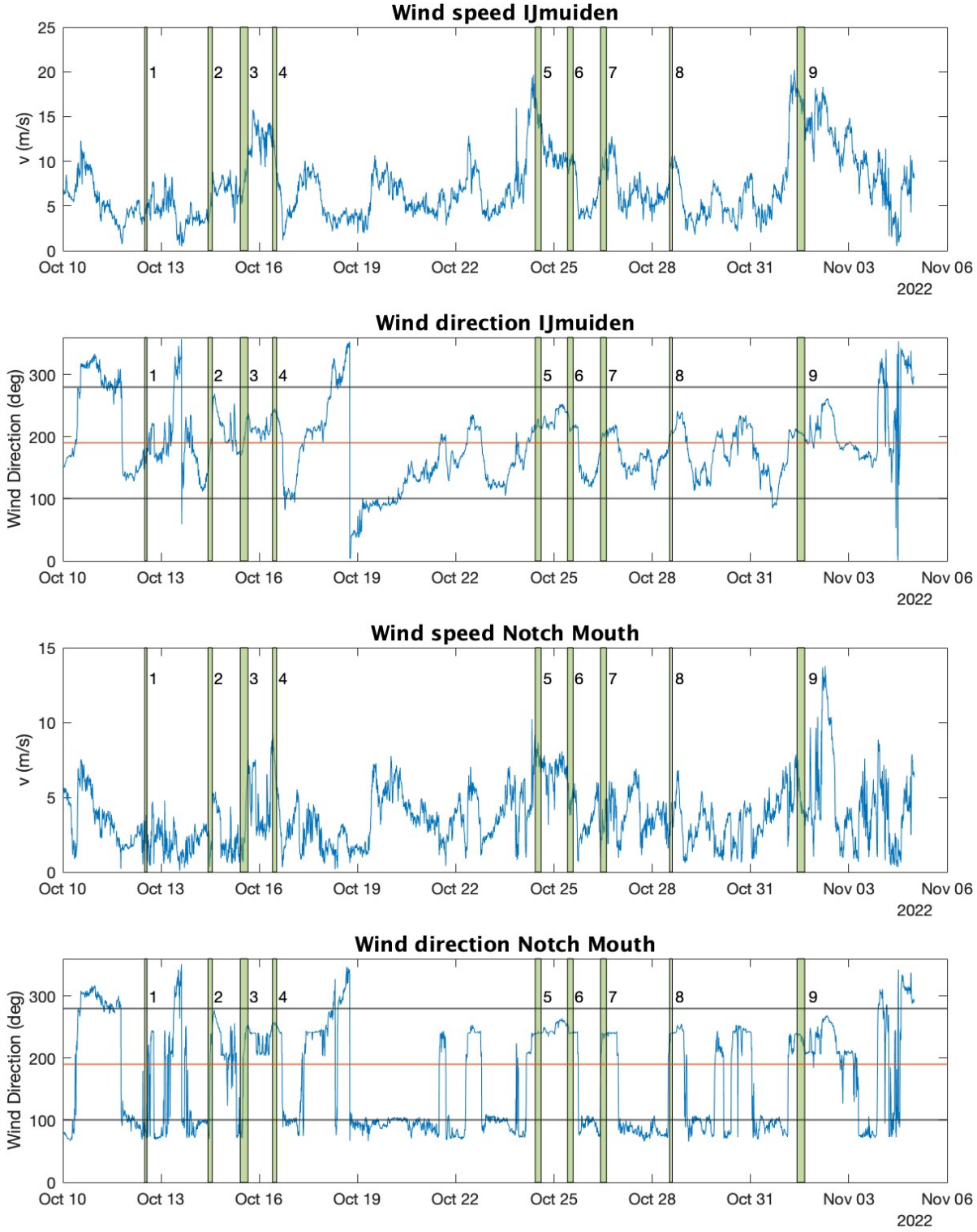

Figure 4.1: Overview wind speed and wind direction in IJmuiden and at the fixed anemometer in the notch mouth. The measurements days are indicated, the notch orientation (black) and perpendicular to the notch orientation (orange).

Very high transport amounts with an almost constant flow of aeolian streamers were seen in the field on day 4, 5 and 9. As Table 4.1 shows, the wind speeds were highest on those days (approach wind speed, IJmuiden, of on average 11 to 17 m/s). Unfortunately, like on day 2 there were some technical issues on day 4. Two SSA did not work properly, therefore only the data from the SSA located in the center on the notch was saved. The approach angle of the wind was slightly oblique on day 4 (Table 4.1: approach wind direction, direction of the wind in IJmuiden, was approximately 240 degrees, the angle between the wind and the notch orientation (280N) was therefore about 40 degrees). While the wind was strongly oblique on day 5 and 9 (Table 4.1: approach wind direction was 205-217 degrees, the angle was therefore between 63 and 75 degrees).

4.2 TEMPORAL AVERAGING INTERVAL

To determine the best temporal averaging interval, the Temporal mean saltation intensity (Equation 2) was plotted over wind speed (Equation 5) for all these intervals (Figure 4.2, green points). In addition, the Temporal mean saltation intensity values were binned for small interval steps for both the TKE and the wind speed. For every 0.2 m/s (0.2 m^2/s^2) interval for the wind speed (TKE) all saltation intensity values that fell within that bin, were averaged into one mean saltation intensity value (binned mean value, Figure 4.2: black points). This was done for every SSA of all the measurement days for six temporal averaging intervals (1s, 10s, 1m, 5 m, 10m and 30m). Furthermore, the standard deviation (SD) between all the temporal mean saltation intensity values within a bin (green points of Figure 4.2) and the binned value (black points of Figure 4.2) was calculated. This SD shows how much the actual saltation intensity values differ from the binned mean saltation intensity value. If the SD is low the spread in actual saltation intensity values is low, whereas the SD is high the spread is also large (Table 4.2).

The SD is smaller for the days with little transport amounts (Table 4.2: day 3, 7, and 8 had on average a SD of ± 7 for 1s, Table 4.2). On the other hand, on days where large transport rates were observed (days 4, 5, and 9), the spread of the saltation intensity values over the wind speed/TKE is large for the smaller temporal averaging intervals (Figure 4.2: the green point cloud has wide distribution and deviates significantly from the binned data for the 1s and 10s on day 5 and 9). Although, a trend can be seen in the binned data, the SD at small temporal averaging interval (1s and 10s) is very high on those days (Table 4.2: SD> 30 for 1s). For the larger temporal averaging intervals (1 min or larger), the saltation intensity values begin to show the same trend as the binned values and the SD decreases significantly (Figure 4.2).

Table 4.2: Standard deviation of the data with the binned data for different temporal averaging intervals, averaged for days with little transport (day 3, 7 and 8) and for days with larger amounts of transport (days 4, 5, and 9).

Days		1 s	10s	1m	5m	10m	30m
Day 3, 7, and 8	**V/SI**	6.3	1.6	0.7	0.3	0.2	0.1
	TKE /SI	7.7	2.0	0.8	0.4	0.3	0.2
Day 4, 5 and 9	**V/SI**	30.3	13.2	7.8	4.1	2.6	1.8
	TKE /SI	38.46	20.0	12.2	5.8	3.9	1.1

Although an improvement in the SD can still be seen at intervals greater than 5-minutes (Table 4.2: for day 4,5 and 9 the SD is decreasing to values lower than 4) a considerable amount of data is lost at those intervals (Figure 4.2: 10 min and 30 min), hence it was decided to exclude 10- and 30-minute temporal intervals.

Ultimately, a discission was made between 1-minute or 5-minutes. Since a 5-minutes averaging interval also contains five times less data than 1-minute, the 1-minute averaging interval was chosen to be used for the remainder of this study. The repercussions of this decision will be examined in greater depth later in the discussion.

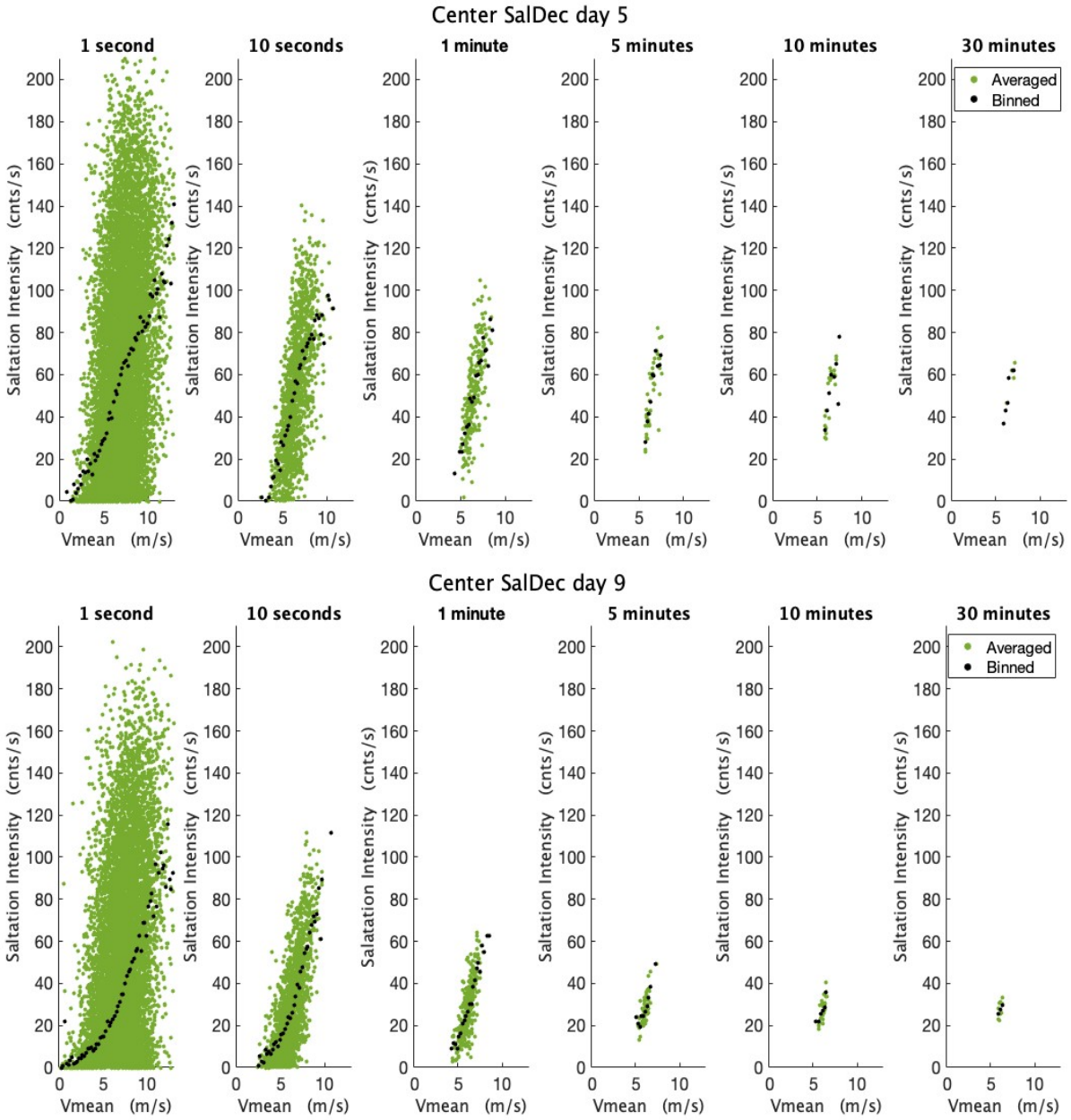

Figure 4.2 Standard deviation of the data and the binned data for different temporal averaging intervals, averaged. Top: SSA in center on day 5; bottom: SSA center on day 9.

4.3 CORRELATION TKE/WIND SPEED AND SALTATION INTENSITY

The binned saltation intensity is plotted against both the wind speed and the TKE for the 1-minute temporal averaging interval (Figure 4.3 and Figure 4.4). On days 1, 2 and 6 (almost) no sediment transport were measured and are therefore not plotted here.

4.3.1 Wind speed

Figure 4.3 shows the saltation intensity over the wind speed. In general, the trend shows that as the wind speed increased the saltation intensity increased as well. The onset of sediment transport started at wind speed of about 4 m/s and increased in an approximately linear fashion. However, there were differences between the different measurement days and locations.

Small transport amounts

For the days with small amounts of transport, there is no clear discernible trend. The onset of transport occurred at different wind speeds visible at every location and/or every day. The best days to see the onset of sediment transport were days 7 and 3 (on day 8 slightly lower saltation intensities were measured). On day 3, the SSA in the center of the notch showed increasing transport rates at higher speeds (Figure 4.3: day 3 center SSA shows increase around 6 m/s). At the northern SSA little to no sediment transport was measured (Figure 4.3: northern SSA day 3). Since it rained extensively in the morning of day 3, the sand was initially wet and therefore may have been difficult to be transported by the wind.

On day 7, sediment transport begins at wind speeds of approximately 4.5 m/s at the southern SSA, while at the other SSA locations sediment transport already seen at lower wind speeds (Figure 4.3: day 7 south vs north and center). Especially the northern SSA shows saltation intensities at much lower wind speeds, about twice as small as the southern SSA (Figure 4.3: day 7, north shows significant increase saltation intensities around 2m/s). The northern SSA (on both days 3 and 7) was positioned in the gully on both days, on day 3 it was located at the beginning of the gully (in the most seaward position), whereas on day 7 it was positioned towards the back/end of the gully (Figure 3.7). The comparatively high saltation in that gully for low wind speeds was also observed on day 9 and will be discussed in detail later.

Higher transport amounts

On the days with larger transport amounts (day 4, 5 and 9), it is more clearly shown that the trends for sediment transport in relation to the wind speed are approximately linear (Figure 4.3: day 4, 5 and 9). On day 5, all three SSA systems followed a similar trend, with southern SSA having slightly higher values on average (Figure 4.3: day 5, South is more the top right of the graph with higher wind speeds and higher saltation intensities). From a windspeed of approximately 3m/s sediment transport was measured and increased in a linear fashion with increasing wind speed. On day 9, the approaching wind speed was the highest on average (Table 4.1: day 9, IJmuiden windspeed was almost 17 m/s) and the wind was most strong oblique (Table 4.1: day 9, wind direction in IJmuiden was 205 degrees, therefore 75 degrees oblique to the notch orientation). Highest wind speeds and saltation intensities have been measured at the southernmost SSA (Figure 4.3: day 9 south). Like on day 7 (and day 3), the northern SSA was placed in the gully (Figure 3.7) and showed a different trend. Figure 4.3 (day 9, north) shows that transport was measured at significant lower wind speeds

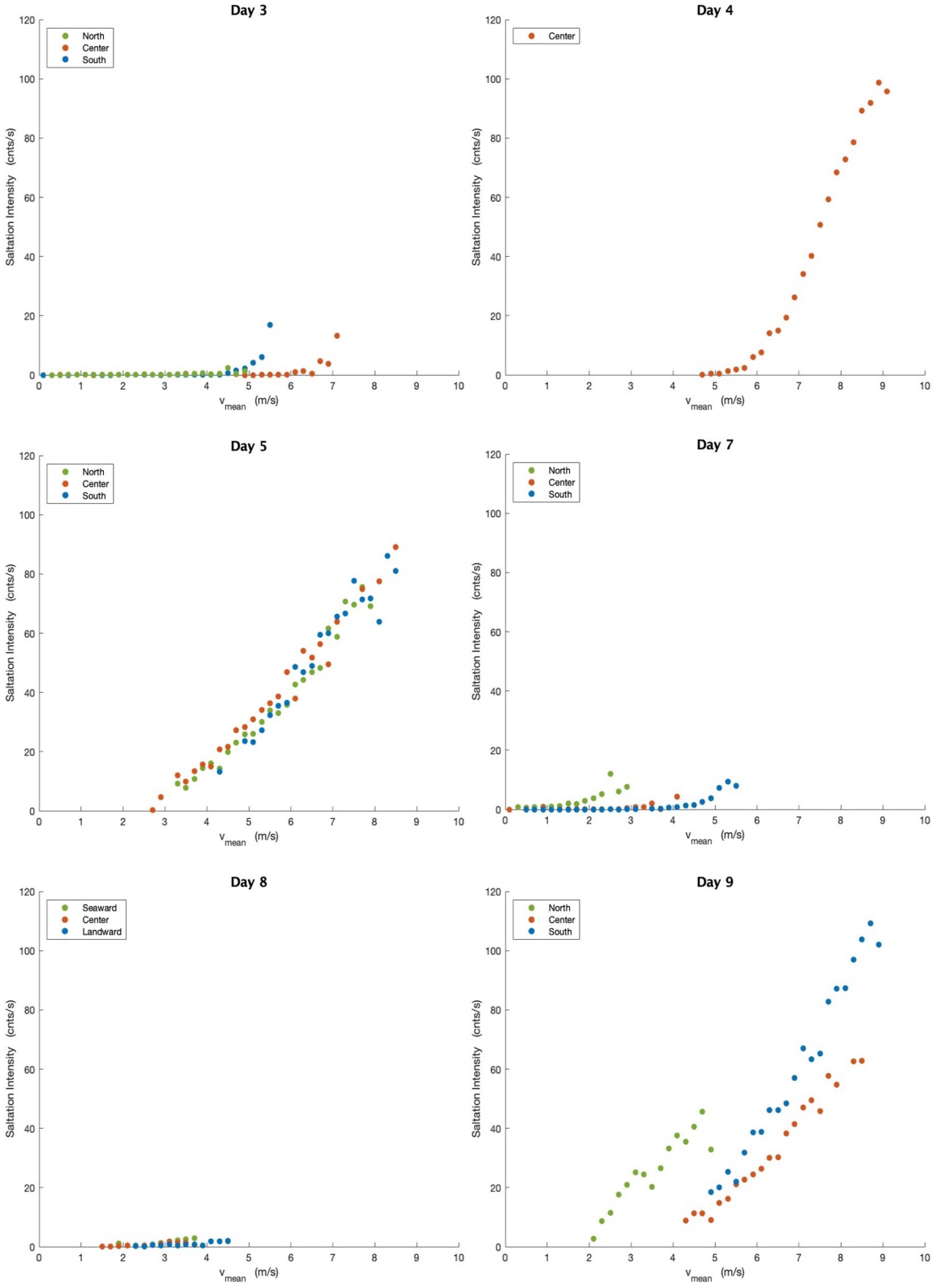

Figure 4.3: shows six plots with the saltation intensity plotted over the mean wind speed for a 1-minute averaging interval.

compared with the other SSA on this day. The threshold for sediment transport is around 2 m/s and the point cloud of the northern SSA is in the lower left of the graph. Although the transport of the northern SSA starts at different location, the slope is approximately the same compared to the other SSAs. Looking in the downwind direction, the SSA was placed in a depression; it is plausible that the wind slowed down here, but the sediment transport due to inertia persisted for a while. On day 4, the approach angle of the wind was slightly oblique (Table 4.1: day 4, wind direction in IJmuiden was 240 degrees, therefore 40 degrees oblique to the notch orientation). Significant amounts of sediment transport have been measured, with values up to almost 100 cnts/s (Figure 4.3: 100 cnts/s for wind speeds of 9 m/s). The wind speed threshold for sediment transport is different than on day 5, transport was only recorded when wind speeds exceed approximately 5.5 m/s (Figure 4.3: day 4), instead of a threshold wind speed of roughly 3 m/s on day 5. Nevertheless, sediment transport rates increase more rapidly, and at speeds of around 8 m/s, the amount of transport is the same as on day 5 (Figure 4.3: on both day 4 and 5 at a windspeed of 8 m/s the saltation intensity is about 80 cnts/s). It rained on the days prior to and in the morning of day 4, but it also rained

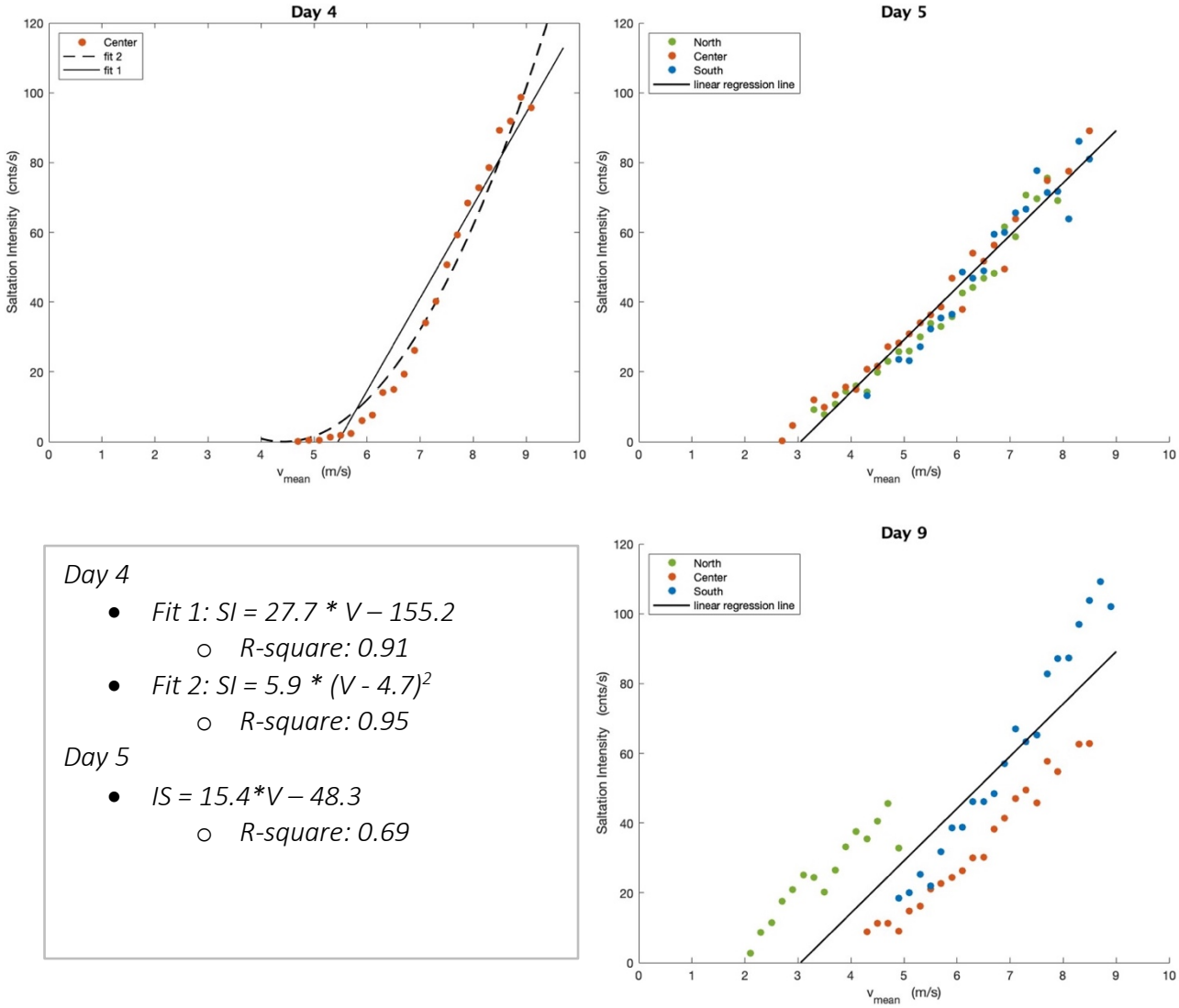

Figure 4.4: Shows the binned data of day 4, 5 and 9 with calculated trendlines. Day 9 shows trend line estimated with data of day 5.

(to a smaller extent) on days 5 and 9. It is hard to tell whether this higher threshold wind speed was dependent on the soil moisture percentage since the later has not been measured.

Since the three SSA were most consistent on day 5, this day was selected to make a trend line first. The trendline was made with the averaged data (Figure 4.2: green points) but are shown here with the binned values. A trendline has also been created for day 4. Since day 4 appears to be a little less linear, two trend lines have been made. The first is a linear function (Figure 4.4: day 4 fit 1), while the second is a parabolic function (Figure 4.4: day 4 fit 2). An exponential fit was also considered; however, it did not fit well. Although the parabolic fit has a slightly higher r-square (0.95) than the r-square of the linear fit (0.91), but the r-square is still relatively high compared to the linear fit of day 5 (0.69) and is therefore still pretty good fit. Figure 4.4 shows the trendlines with binned data. The slope of the linear trendline on day 4 is almost twice as large as the slope on day 5 (Figure 4.4: slope of 27.7 on day 4 and 15.4 on day 5). The two trendlines are also plotted with the data of day 9. It seems that slope of day 9 is right in between that of day 4 and 5 but show a different threshold for sediment transport. The threshold is most different for the northern SSA on day 9.

4.3.2 Turbulent kinetic energy

Figure 4.5 shows the saltation intensity over the TKE. In general, the saltation intensity increases with an increasing TKE. However, the trend is less constant and the differences between the days and locations are much greater for TKE than they were for the wind speed.

Small transport amounts

On the days with small amounts of sediment transport an increase in saltation intensity could be seen at a TKE of more than 2 m^2/s^2 (Figure 4.5: days 3, 7 and 8). The southern SSA, both for day 3 and day 7, indicated the greatest increase in saltation intensities with rising TKE (Figure 4.5: day 3 and 7, south shows stronger increase from 2 m^2/s^2 than center and north). The other SSA on day 3, did not show much of an increase in saltation intensities under rising TKE values (Figure 4.5: day 3 center and north). On day 7, the saltation intensity also grew with an increasing TKE for the other SSAs, but the onset of transport starts at a higher TKE (Figure 4.5: day 7, center and north shows stronger increase from 2.5-3.0 m^2/s^2). Since the little saltation intensity quantities, no clear correlation can be withdrawn between the saltation intensity and TKE for these days. However, in general, the saltation intensity increased as the TKE increased.

Higher transport amounts

During very oblique winds (day 5 and 9) the data from the three SSA systems showed a less apparent correlation in the graph of the saltation intensity over the TKE appears than for the wind speed. However, as the TKE grew, the saltation intensity increased as well, but the growth rate and degree of dispersion differed depending on the measurement location. There are two distinguished groups here: the SSA located in south of the notch and the SSAs in the center and north. The saltation intensity increases relatively fastest with increasing TKE at the southernmost SSA. The trend is steeper than the trend at the other two locations (Figure 4.5: day 5 and 9, south vs center and north). On day 5, the saltation intensity increased from 40

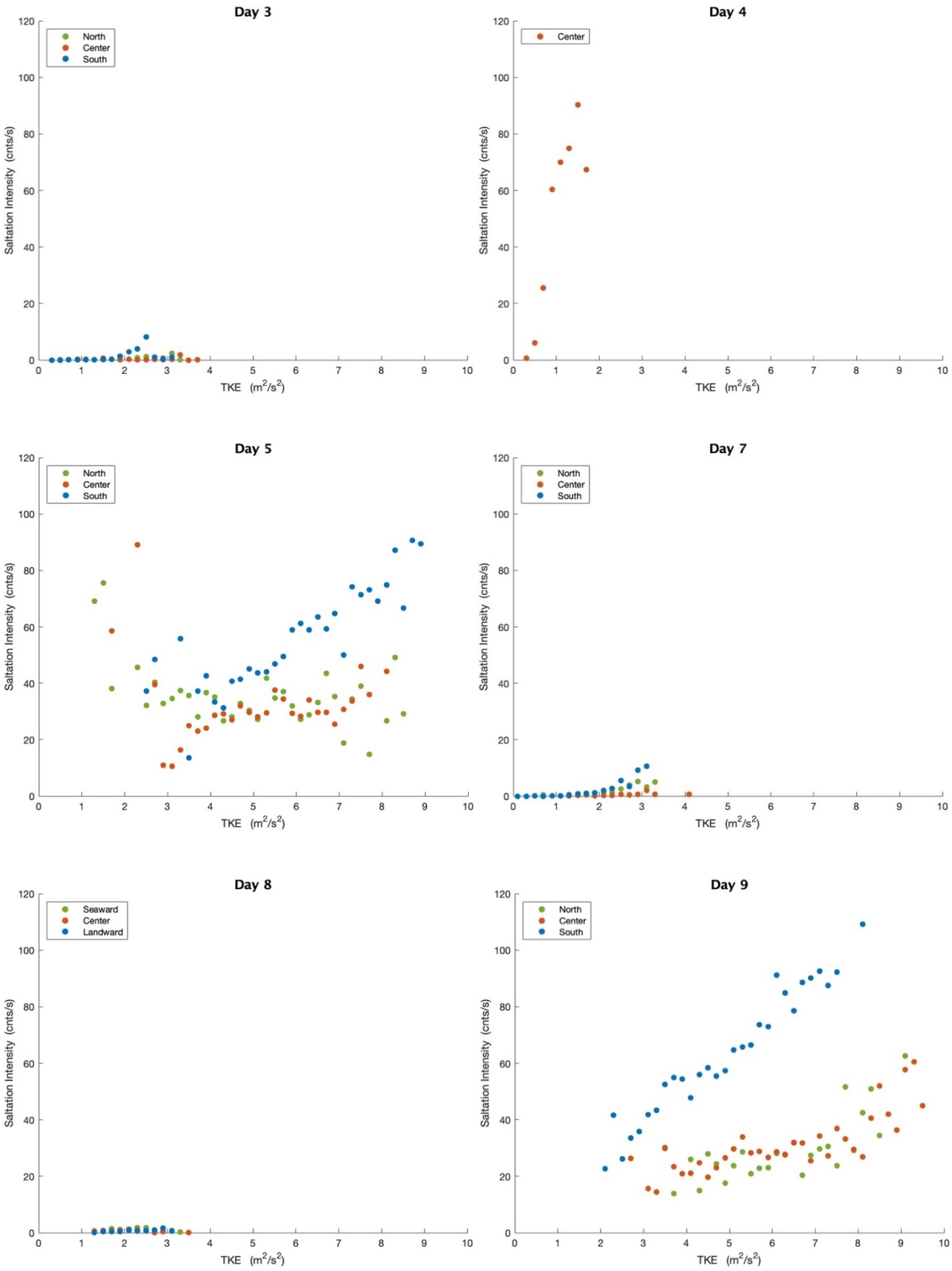

Figure 4.5: Shows six plots with the saltation intensity plotted over the TKE for a 1-minute averaging interval.

cnts/s to 90 cnts/s as the TKE increased from 5 m^2/s^2 to 9 m^2/s^2 (Figure 4.5: day 5), resulting in a slope of about 12.5. The slope is similar to the slope of day 9, but on day 9 the onset starts at a lower TKE (Figure 4.5: day 9 south, saltation intensity is increasing from 40 cnts/s to 90 cnts/s as the TKE increased from 3 m^2/s^2 to 7 m^2/s^2). The SSA in the center and north shows a much lower slope for saltation intensity and TKE, between 3 and 7 m^2/s^2 the saltation hardly seems to increase (Figure 4.5: day 5 and 9, north center). On day 9, when TKE becomes greater than 7 m^2/s^2, the saltation intensity increases more significantly (Figure 4.5: day 9, north and center). On day 4, the approaching wind was slightly oblique (Tabel 4.1: 40 degrees). The TKE remained relatively low (smaller than 2 m^2/s^2) while high saltation intensities were reaches (larger than 90 cnts/s). The slope for saltation intensity and TKE is much steeper (Figure 4.5: day 4).

In general, Figure 4.5 shows that the saltation intensity increased, with an increase in turbulence (TKE). However, the rate of increase is not similar for all days and all locations; on the contrary, there are considerable differences. It is therefore not possible to attribute a predictive value for sediment transport given the TKE.

4.4 COEFFICIENT OF VARIATION

4.4.1 Coefficient of variation of the wind (cv_k) and saltation intensity

The coefficient of variation of (or turbulence intensity relative to) the wind speed is calculated by dividing the square root of the TKE by average wind speed. The temporal coefficient of variation (or relative standard deviation) for wind speed (CVk) was plotted against saltation intensity (Figure 4.6).

The coefficient of variation of the wind speed (CVk) reached high values on the days with little transport amounts (day 3, 7 and 8). Because the values on days 3 and 7 deviated considerably from the CVk values on the other days, it was decided to plot CVk over the saltation intensity with different axis limits than the other days (Figure 4.6: day 3, 7 and 8). On day 7, the CVk is especially high for the northern SSA which was located in the gully (Figure 4.6: day 7, notch gives values up to 700%), there was relatively a lot of turbulence for the magnitude of wind speed. It was significantly different from the other SSAs that day, which had CVk values up to roughly 80% (Figure 4.6: day 7, north and center). On day 3, the CVk values were also very high, especially for saltation intensity values of zero (or slightly bigger than zero, Figure 4.6 day 3). Therefore, it can be said that the CVk can be quite high under low transport conditions. However, generally the spread the magnitude of CVk reduces as saltation intensity increases.

On days 4, 5, and 9, some SSAs had relatively constant values of the CVk values for all saltation intensities, hence the CVk values against the saltation intensity were roughly plotted as a horizontal line. This was the case for the southern SSA on day 5 and 9 and for the central SSA on day 4 (Figure 4.6: south of day 5 and 9, center day 4). However, the CVk value, and hence the height of this 'horizontal line', varies between these three days. The value was lowest on day 4 (Figure 4.6: day 4 CVk value of approximately 10%), indicating that the TKE was modest in relation with the magnitude of the wind speed. The CVk was slightly lower on day 9 (Figure 4.6: day 9, south had CVk value of 30-35%) than on day 5 (Figure 4.6: south had CVk value of 35-40%).

On day 5, the other two SSA showed a declining trend with the saltation intensity increased as the CVk decreased. The saltation intensity gradually increased with rising wind speeds, whereas it remained relatively constant for an increasing TKE (Figure 4.3 and 4.5: day 5). The

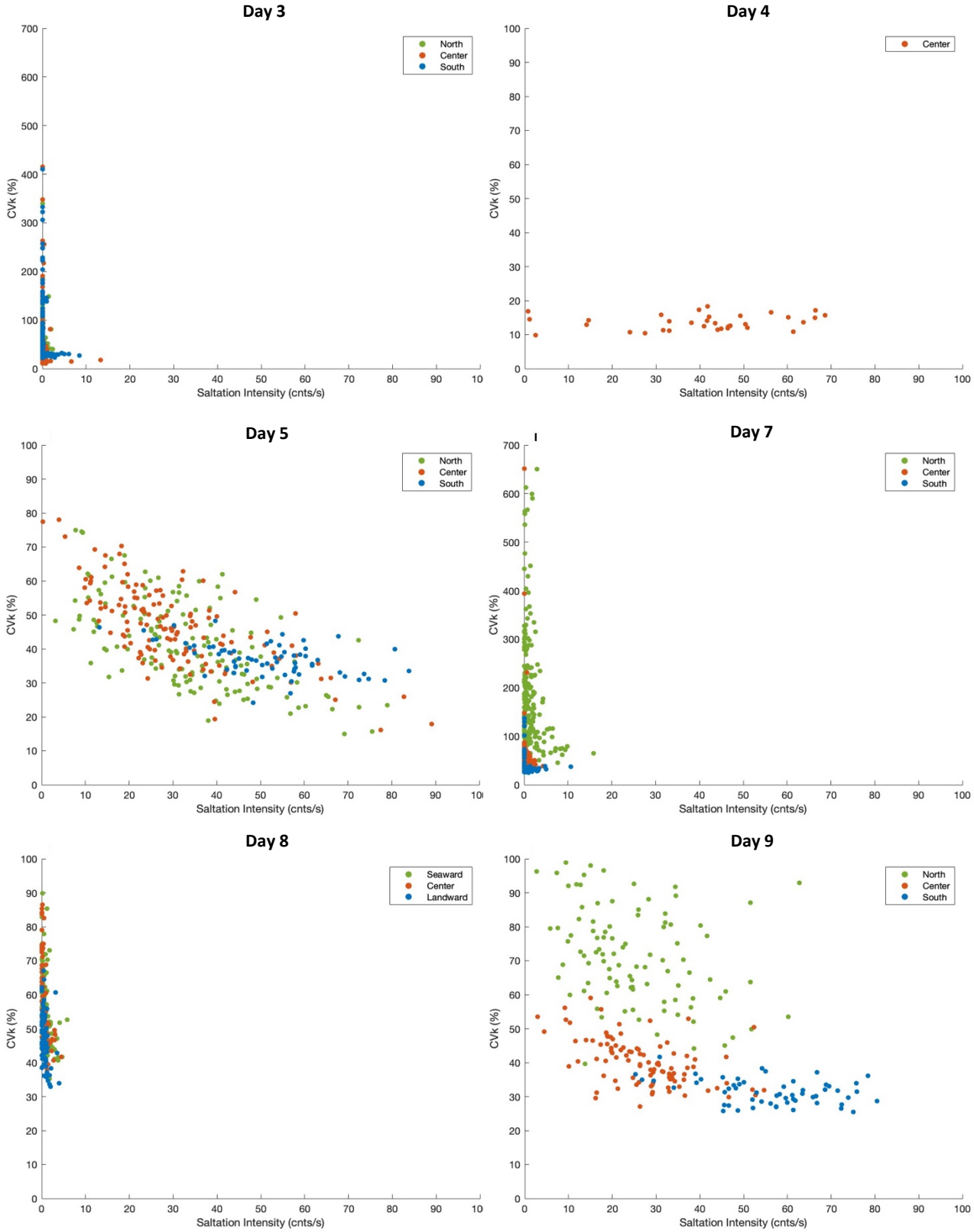

Figure 4.6: Shows six plots with the coefficient of variation against the saltation intensity for a 1-minute averaging interval.

sediment transport is more depended on the wind speed than on the turbulence here and therefore for a rising saltation intensity, the coefficient of variation of the wind speed decreased (Figure 4.6: day 5). On day 9, the central SSA showed less scatter than the two SSAs (center and north) on day 5. The points are more clustered and saltation intensities increased as the CVk decreased (Figure 4.6: day 9, center). Contrarily, northern SSA on day 9 differed as it was located significantly more towards the top right of the plot, where the CVk was relatively high and the saltation intensity low. This indicates that it was relatively turbulent compared the wind speed (Figure 4.6: north day 9).

On the basis of this data some general observations can be made. One could argue that the sediment transport increased on average with a declining CVk. However, trends are not apparent enough to make reliable predictions. At lower saltation intensities (<40 cnts/s) there is great variation in the CVk (can be both high and low: between 20% and 700%), while for higher saltation intensities (larger than 60 cnts/s) the CVk is often relatively low (smaller than 40%). Low CVk values (smaller than 50%) do not necessarily indicate a lot of sediment transport, whereas at high transport values (larger than 50 cnts/s) it is unlikely that the CVk values will be greater than 50% (Figure 4.6).

4.4.2 Coefficient of variation of the wind (CV_k) and of the saltation intensity (CV)

In general, these plots show that when the the CVk grows, the coefficient of variations of the sediment transport (CV) increases as well. For days with little transport (days 3, 7 and 8), high values for the CV up to almost 6000% (Figure 4.7: day 3, 7 and 8). Therefore, different limits have been used for the axis for these days than for days with higher transport rates.

The SSA that showed a roughly straight horizontal line in CVk against saltation intensity plots (Figure 4.6) are also nearly constant in CVk values in these plots (Figure 4.7: center on day 4, South on day 5 and day 9). The relative gustiness of the wind (i.e., Coefficient of variation of the wind, CVk) appeared to be more constant than the fluctuations in sediment transport (CV). For the SSAs located in the gully at the north (northern SSA on days 7 and 9), the CVk is relatively large in comparison with the fluctuations in transport (CV). This might be as a result of the morphology that was previously discussed, which causes changes in the wind while sediment is transported a little further because of inertia.

Furthermore, most other SSA show that as the gustiness of the wind increased (higher CVk) the fluctuations in transport (CV) also become larger. However, there is no (to almost no) clear relation between the coefficient of variation of the wind and sediment transport.

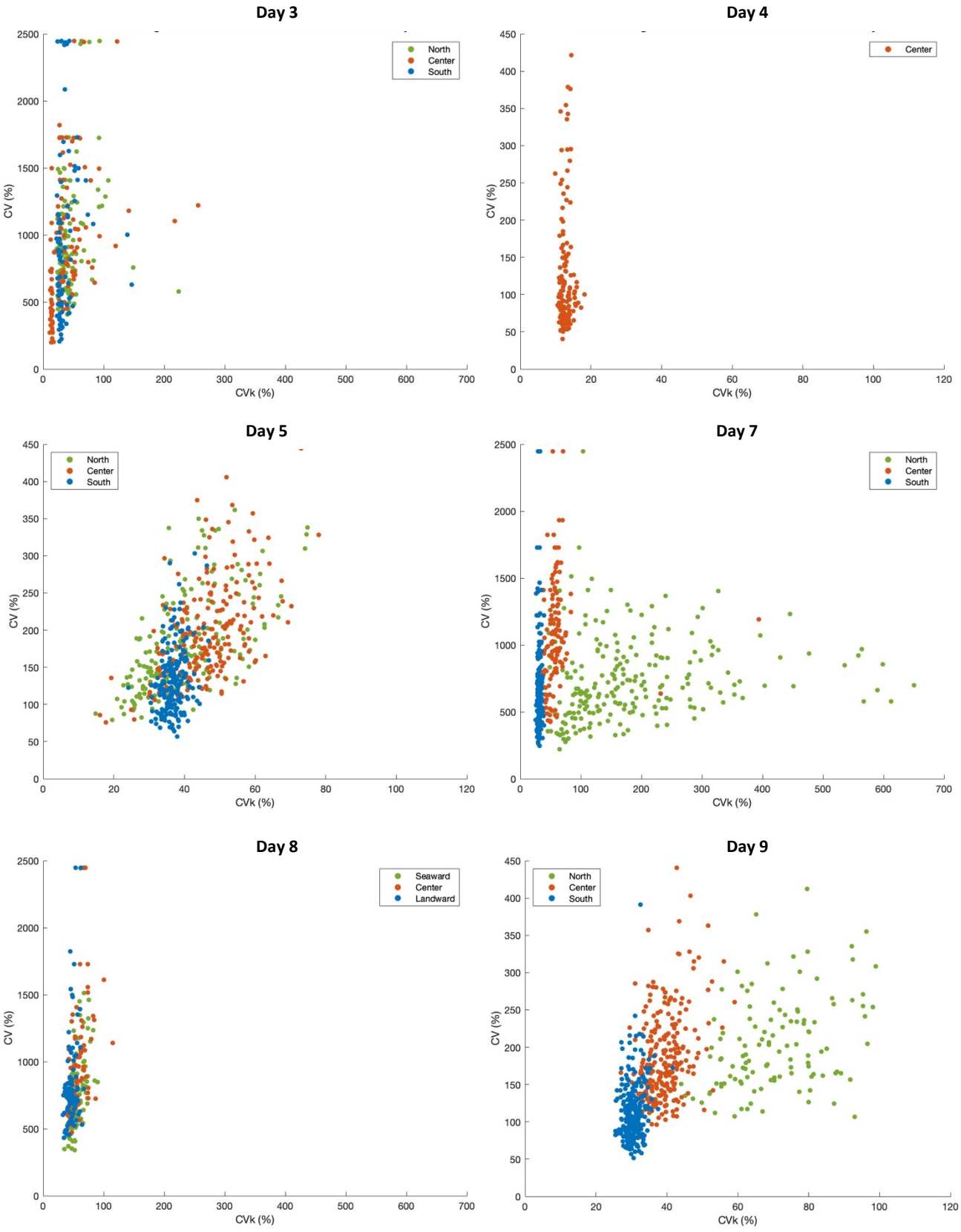

Figure 4.7: Shows six plots with the coefficient of variation of the salutation intensity against coefficient of variation of the wind for a 1-minute averaging interval.

4.5 SPATIAL VARIATIONS AND APPROACH ANGLE OF THE WIND

During the fieldwork, southwesterly winds were dominant and there were no measurement days with wind from the west or even northwest. This makes it difficult to obtain a thorough understanding of the spatial variation under various approach angles of the wind.
As can be seen from the wind roses of the four fixed anemometers in the notch, the wind in the notch has only two dominant directions. The wind is altered to either enter or exit the notch (Figure 4.8). The wind in IJmuiden comes shows large variations in the wind directions (Figure 4.1: wind direction in IJmuiden and Figure 3.3: the wind rose of IJmuiden), while the variation is substantially less in the notch (Figure 4.1: wind direction mouth of notch). When the wind in IJmuiden was approximately perpendicular to the notch orientation, 190N, the wind at the fixed anemometer tends to change 180 degrees with slight fluctuations in approach angle of the wind, switching from blowing in (out) to blowing out (in) of the notch. On the 22nd and 31st of October, the wind at IJmuiden had small fluctuations, whereas the wind in the notch frequently changed 180 degrees (Figure 4.1).

The top plot of figure 4.9, depicts the coefficient of variation of the wind (CVk) for the fixed anemometer (SA02) over the wind direction in IJmuiden, indicating how the relative turbulence changes under different wind approach angles during the fieldwork. The black lines in the plot indicate the orientation of the notch (100N and 280N), thus if the wind is parallel to the notch orientation. The orange lines indicate the direction that is perpendicular to the notch orientation (10N and 190N). The relative turbulence increased as the angle between the notch orientation and the wind increases. When the wind was more oblique than approximately 50 degrees from the notch (Figure 4.9: top, angles between 150 and 230N) the airflow becomes relatively more turbulent, with the CVk being maximum when the wind was approximately perpendicular to the notch (Figure 4.9: top, 190N). The bottom plot of figure 4.9 shows the relative wind speed at a fixed anemometer (wind speed at a fixed anemometer divided by the wind speed measured in IJmuiden) against the wind direction in IJmuiden. This shows that as the angle relative to the notch orientation increased, the relative wind speed in the notch decreased. When the approach wind was very oblique, the wind was less effectively steered and accelerated through the notch than for less oblique winds. The relative speed became significantly smaller at the same wind directions where CVk increased, thus under oblique wind with angles larger than ±50 degrees relative to the notch orientation.

The values (CVk and relative wind speed) for the measuring days are also plotted in Figure 4.9. The wind was substantially more oblique on day 5 and 9 (63-75 degrees) than on day 4

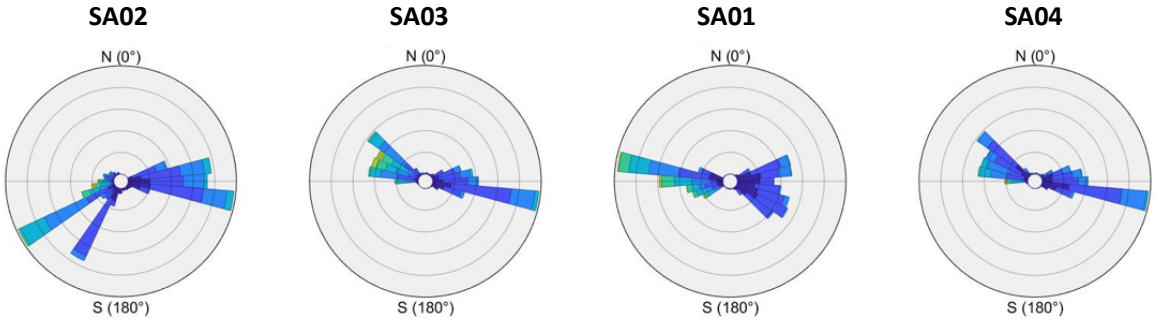

Figure 4.8: Wind roses of the four fixed anemometers in N2 during the fieldwork

(40 degrees). Therefore, the wind on day 4 had a lower CVk (10%) and the relative wind speed was quite high (0.7). As the wind came more oblique (day 5 and even more oblique on day 9) the CVk increased (Figure 4.9: CVk on day 5 and 9; 20% and 40%), while the relative wind speed decreased (Figure 4.9: relative windspeed on day 5 and 9; 0.5 and 0.4). Figure 4.5 also showed that on day 4 the TKE was significantly lower than on day 5 and 9.
Although the wind speed decreases and the CVk increases when the wind becomes more oblique to the notch orientation, the wind direction will still be realigned to notch orientation due to topographical steering.

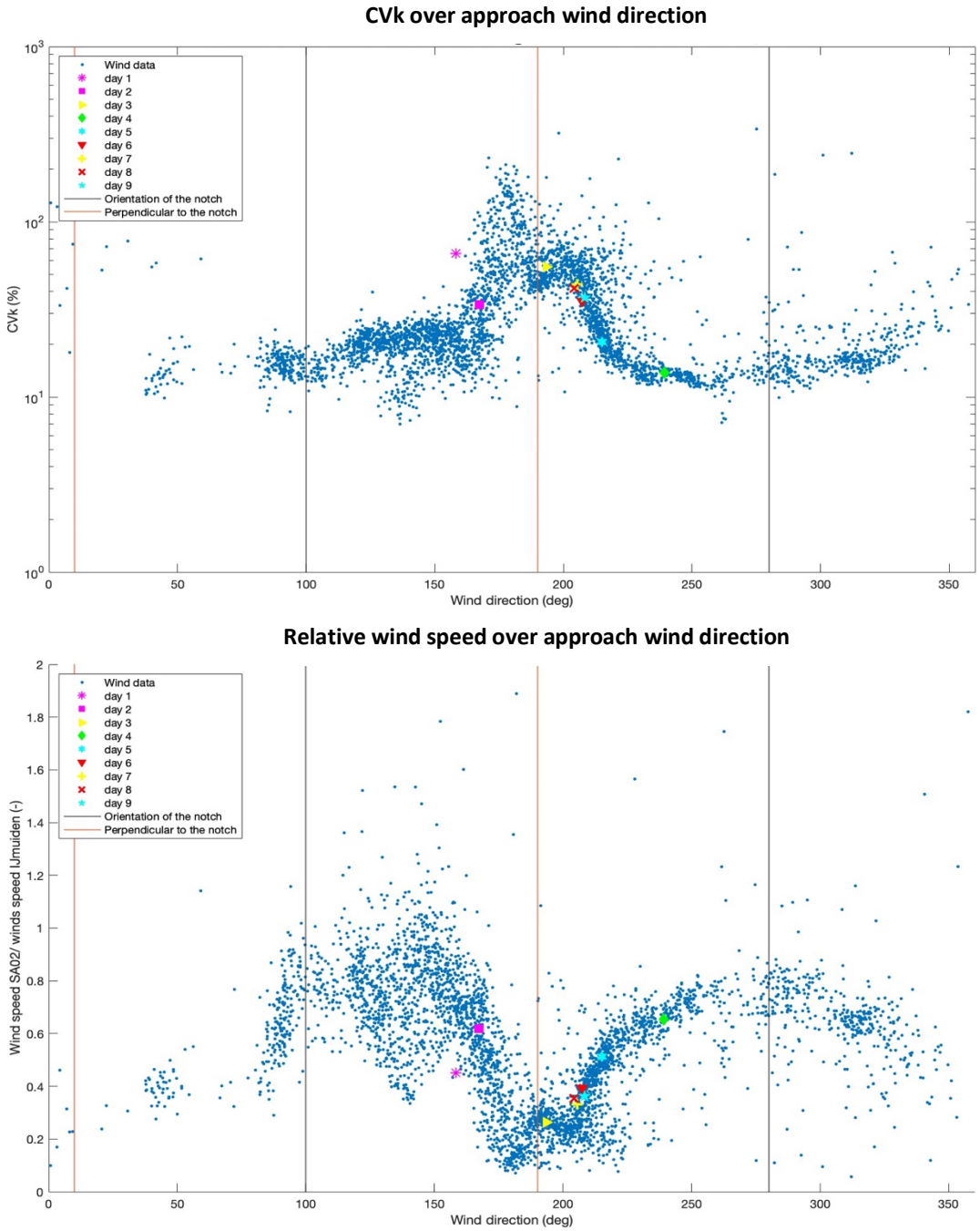

Figure 4.9: Wind characteristics in the mouth of the notch as function of the wind direction in IJmuiden. Top: the CVk over the wind direction in IJmuiden, bottom: the relative wind speed at a fixed anemometer (wind speed at a fixed anemometer divided by the wind speed measured in IJmuiden) against the wind direction in Ijmuiden. Black lines: notch orientation, orange lines: perpendicular to the notch orientation.

5. DISCUSSION

5.1 TEMPORAL AVERAGING INTERVAL

Like the study of Smyth et al. (2014), this study also found that the correlation between sediment flux and wind parameter became more apparent as the averaging interval was raised. The study of Smyth et al. (2014), only compared 10-second and 1-minute averaging intervals, whereas in this thesis various time averaging intervals (1s, 10s, 1m, 5m, 10m, 30m) were examined.

The best temporal averaging interval was selected as one of the initial processing steps and was used to provide the other results. The 1-minute averaging interval appeared to be the best option. The distance between the SalDec and the sonic anemometer undoubtedly has a role in determining the best time averaging interval. The sonic anemometer (SA) was typically located approximately 0.8 m from the middle of the SalDec (the SalDec is 0.8 m wide and to ensure that the sediment transport is not disturbed, the SA is not placed directly next to the SalDec). In addition, the SalDec measured the sediment transport at 0.1m above the ground, while the Sonic anemometer measured the wind at about 0.9m. There are many different types of turbulence, including small eddies in the internal boundary layer that generate streamers; these little turbulences are very local and may not be observed properly at a height of 0.9m. The best averaging interval is influenced by the measuring distance, it determines the size of the eddies that can be observed while there is also a correlation between that eddy and the sediment transport Ellis & Sherman (2022).

The question is whether the results would have been significantly different if a different averaging interval had been used. This is not the case; the linear regression line for windspeed and sediment transport (of day 5) obtained with the 10-second and 5-minute averaging interval is similar to the trend calculated at the 1-minute averaging interval (Figure 5.1: slope of 15.38 for 10s and 14.99 for 5 min vs 15.35 for 1 min). The expectation is that as the averaging time increases, the R-square would also increase, which is indeed the case, but the differences are small (Figure 5.1: R-square, 0.60 for 10 s; 0.76 for 5 min vs 0.69 for 1 min). Despite some small differences, the results and patterns are quite similar for 10-seconds, 1-minute and 5-minutes averaging intervals. However, the linear regression line of 1-minute and 5-minutes averaging intervals are more similar than one calculated for the 10 second averaging interval. Additionally, the standard deviation was larger for the 10-seconds interval (Table 4.2: e.g., wind speed (day 4, 5 and 9) had SD of 13.2 (10 sec) and 7.8 (1-min)), indicating that the differences between averaged data and binned values was also much larger. Between 1 and 5 minutes the difference is smaller, but there is less data that remains available when 5 minutes is used. Taking all of this into consideration, the decision to use one minute as the averaging interval for this study was appropriate.

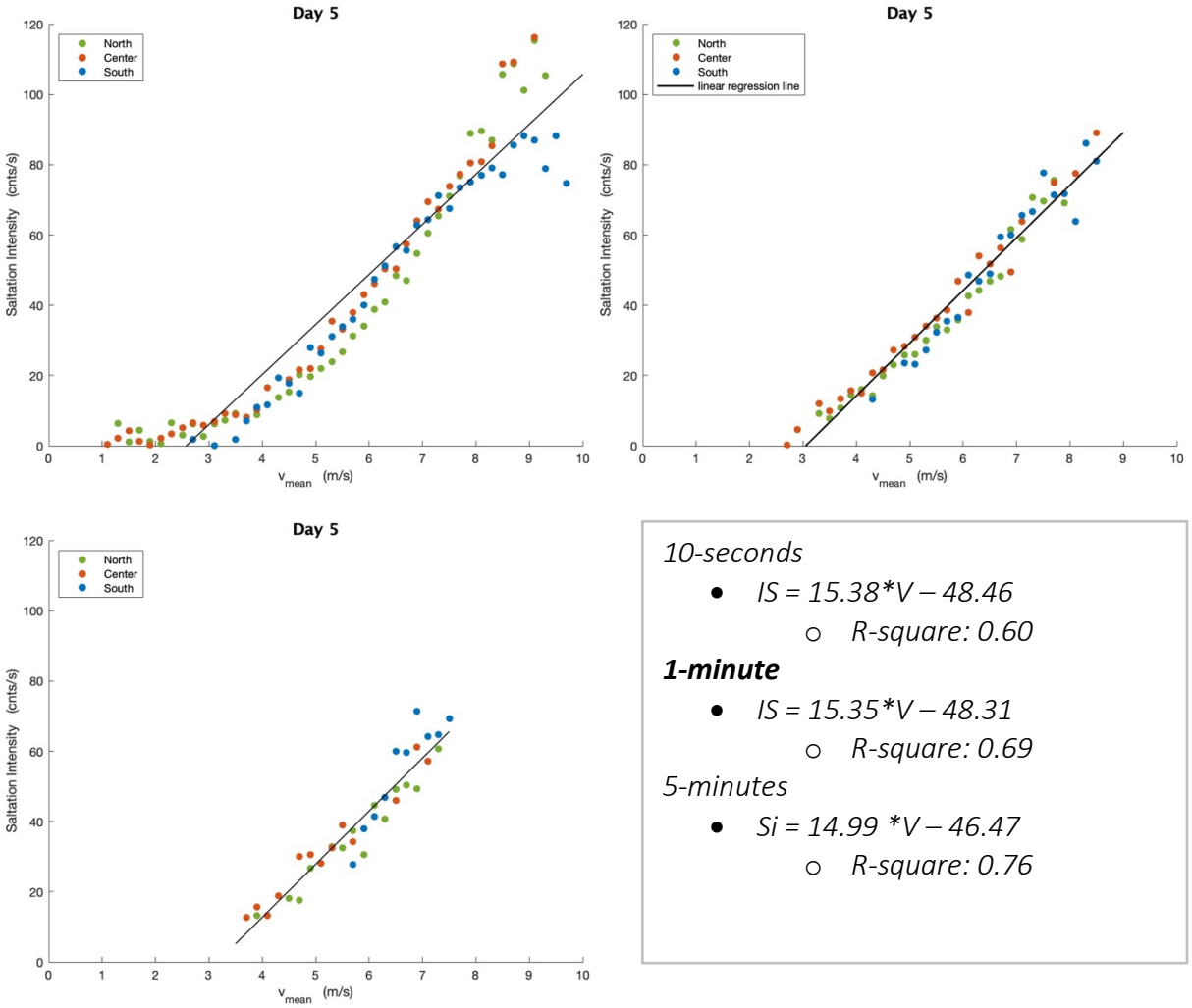

Figure 5.1: Data and trendline for different temporal averaging intervals. Top left: 10s, top right: 1-minute, bottom left: 5-minutes

5.2 AEOLIAN SEDIMENT FLUX

At minute scale averaging intervals, Smyth et al. (2014) discovered that TKE, may be a stronger predictor of sediment transport than wind speed. This does not apply for this study; the TKE does not provide a better trend than the wind speed, nor does it improve for larger time averaging intervals. Turbulence occurs at a variety of magnitudes where the spatial and temporal scales are linked. Because the wind and sediment transport sensors were positioned quite far apart (see chapter 5.1, about 1.0 meter apart and at height difference of 0.8m), this research automatically focussed on the larger turbulent eddies (60-100s scale). In the study of Smyth, the sand trap and the Sonic anemometer were positioned at 0.5 meters above the surface and were 0.5 meters apart. Therefore, those measurements were made at a closer distance than during this study. That could explain why Smyth et al. (2014) found a better correlation for the TKE than was found during this study. A recent study of Ellis & Sherman (2022) discovered a very strong relationship between small scale turbulence and sediment transport, especially on a very short time scale (<2s). The study was conducted on various beaches with a significant fetch. The measurement conditions and settings were very

different setting than this study, however the results are noteworthy. During the study, measuring equipment was positioned very close together and near the surface (20-40 mm apart and 10-40 mm above the bed). It was therefore possible to investigate small-scale structures, as the wavelet analysis.

In this study, wind speed gave the best correlation for sediment flux and the dependency is approximately linear. This is in contrast with traditional studies that found that 3rd power models provide a better correlation for sediment transport than simply wind speed when analysing data in a subsequent study. Nevertheless, research of de Vries et al. (2014) found that a linear formulation can be an alternative to traditional third power models. Especially under supply limited conditions the linear model fitted the data best. The linear model is less dependent on variability in the wind speed and emphasizes the importance of supply rather than the importance of wind speed (De Vries et al., 2014). The linear trend found in this study confirms the findings of De Vries et al. (2014).

Nevertheless, there were significant differences between these correlations for wind speed at various locations and on the different measurement days (boundary conditions). On day 4 with slightly oblique winds (40 degrees) the onset of sediment flux started at high wind speed (Figure 4.3: day 4 onset at 5.5 m/s), for which no clear explanation was found during this study. However, the slope between sediment transport and wind speed was greater (Figure 4.4: day 4 slope of 27.7), therefore at higher windspeeds the transport rates were similar (Figure 4.4: day 4 and 5, at 8 m/s, saltation intensity of 80 cnts/s). During strong oblique winds (day 5 and 9: 63 and 75 degrees) the slope was twice as small as on day 4 (Figure 4.4: day 5 had slope of 15.4 vs a slope of 27.7 on day 4), but the onset of sediment transport started at a lower wind speed (Figure 4.4: day 5 and 9 between 3 and 4 m/s, except for the Northern SSA on Day 9). In general, sediment transport starts at a wind speed between 3 and 5.5 m/s and the saltation intensity increases with a slope between 15 and 30 times the wind speed.

The TKE is less suitable given the large degree of scatter and lack of systematic trend. TKE increased as the wind became more oblique (Figure 4.5: day 4 vs day 5 and 9), but the trend was less consistent than it was for wind speed. During less oblique winds, the TKE was lower and showed a steeper slope for the saltation intensity (Figure 4.5: day 4: TKE between 0 and 1.5 m^2/s^2, saltation intensity rises from 0 to 90 cnts/s -> slope of 60). During very oblique winds, for different TKE values saltation intensities remained approximately constant especially in the north and center of the notch (Figure 4.5: day 5 and 9, center and north: TKE between 1 and 9.5 m^2/s^2, saltation intensity values between 0 to 60 cnts/s -> slope of 7). The southern SSA gave a stronger increase in saltation intensity with rising TKE values (Figure 4.5: day 5 and 9, South: TKE between 2 and 8 m^2/s^2, saltation intensity rises from 0 to 120 cnts/s -> slope of 20).

Smyth et al. (2014) found a negative relationship between coefficient of variation of the wind speed (CVk) and sediment flux. During this study the CVk and saltation intensity did not give a constant trend. Although in general the saltation intensity decreased as the CVk increased, there are exceptions where this was clearly not the case (Figure 4.6: e.g., day 4, and south of day 5 and 9). In addition, the coefficient of variation of saltation intensity (CV) generally increased as the variation in the CVk increased, but again there were exceptions (Figure 4.7:

e.g., day 4, and south of day 5 and 9). The CVk is therefore not suitable to use as a predictor of saltation intensity (both absolute saltation intensity values and CV).

5.3 SPATIAL VARIATION

As shown in Figure 4.3 (days 7 and 9), the correlation between wind speed and sediment transport for the northern SSA deviates when placed in the gully (days 7 and 9). The wind speed is relatively low for the saltation intensities and sediment transport starts at 2 m/s (instead of at 3 m/s or higher, Figure 4.3). This is most likely due to the gully acting as a local depressive, causing the wind to decelerate significantly. The sediment presumably still had some momentum and therefor persisted moving for a while. However, a lot of sediment has been deposited in the gully, as can be seen on the difference map from the fieldwork (Figure 5.3). Even though, high saltation intensities had been measured in the gully, the wind speed decelerated to the point where that sand was deposited.

Smyth et al. (2014) found that the correlations (between sediment flux and wind parameters) were strongest in the centre of the blowout and weakest close to the erosional walls. However, this study showed that during oblique winds (days 5 and 9), the SSA located in south of the notch measured on average the highest wind speeds, the lowest TKE values and the greatest transport rates (Table 4.1, Figure 4.3 and 4.4: day 5 and 9, south). Additionally, the wind direction was altered most there (Table 4.1: south day 5 and 9). The results of Smyth et al. (2014) might be true during parallel wind, but those conditions have not been measured during the fieldwork. In the south, the wind seemed to be steered along the southern erosional wall, altered, and accelerated. In the center and north of the notch, the wind is less steered and blowed more straight into the notch, resulting in more turbulence as the wind reached the northern erosional wall (Figure 5.2). The wind followed different pathways rather than moving as a uniform sheet through the notch. The Figure (5.2) also shows that as the wind exits the notch, it deflects even further along the southern erosional wall, a process seen in the field.

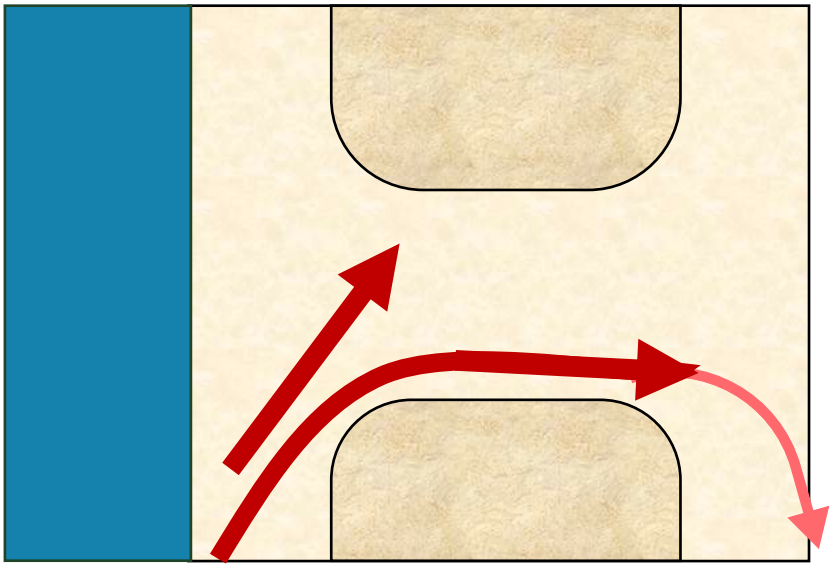

Figure 5.2: Schematic overview pathways that the wind follows during very oblique winds

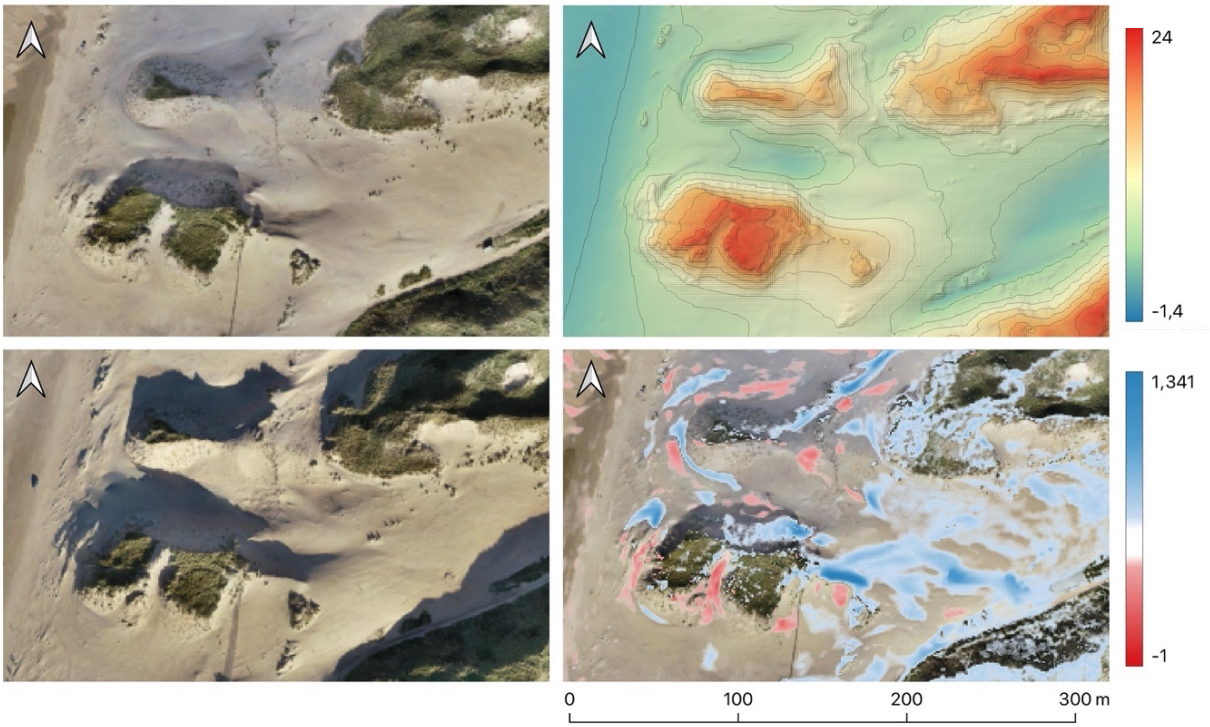

Figure 5.3: Overview of changes in the study area during the field work. Top left: aerial photo at the start of the field work, bottom left: aerial photo at the end of the field work, top right: DEM at the start, bottom right: differences between DEMs at start and at the end of the fieldwork. Legend is in m MSL. *Data used extracted from DOI 10.5281/zenodo.7010095*

Nguyen (2022) discovered that flow streamline compression, wind realignment, and acceleration did not occur at angles greater than 27 degrees. Pease and Gares (2013) discovered, as the approach angles became more oblique to the blowout axis, the wind flow is forced to ever greater amounts of realignment and therefore the rate of steering increases. At an angle greater than 50 degrees to the axis of the blowout, the wind was no longer steered into the blowout but instead flows perpendicular to the axis, across and over the blowout. Smyth and Hesp (2016) found that from a range of oblique angles (angles of 45 degrees) will be steered along the axis of blowout, but no near surface jet is formed. However, when compared to axis parallel wind flows of the same incident wind speed, the relative effectiveness of eroding and transporting sediment outside the deflation basin and erosional walls is reduced significantly.

Figure 4.9 top, indicates that the CVk not only increased as the wind became more oblique (angles greater than 50 degrees), but that the spread in CVk values increased as well. For angles smaller than 50 degrees, the CVk appeared to be very steady and usually had values between 10 and 20% (Figure 4.9). The relative wind speed in the notch (wind speed SA02/ wind speed IJmuiden) also decreased as the angle between approach wind direction and notch orientation increases (Figure 4.9: bottom from about 0.7 to 0.4). When the wind becomes more oblique (greater than 50 degrees), the wind becomes relatively more turbulent, shows a greater spread and the relative wind speed decreases in the notch. Since predominant wind direction was south/southwest during the fieldwork, its it difficult to

determine if the same mechanisms will appear when the wind is oblique from the north/north-west. The wind direction at Ijmuiden is significantly more variable than the wind measured at the fixed anemometer in the notch mouth (SA02), the predominantly wind direction is either orientated in or out the notch (Figure 4.1). The wind roses of the notch confirm this idea and show that the wind only comes from two dominant directions (Figure 4.8). In contrast with Nguyen (2022) and Pease and Gares (2013), this study showed even during very oblique angles of wind was steered along the axis of the notch (up to 75 degrees on day 9). Even though the wind in the notch becomes more turbulent and has relatively lower wind speed when the angle is greater than 50 degrees, the notch can steer, realign, accelerate very oblique winds. Additionally, high transport values have been measured during very oblique winds, the notch is still capable of transporting sediment, at least under south-westerly wind conditions in the mouth of the notch. The observations of this study thus agree with what Smyth and Hesp (2016) found. Sediment transport has not been measured in the deflation basin and on the depositional lobe of the notch, it is however plausible that the notch is less effective in transporting sediment when the wind become more oblique, as Smyth and Hesp (2016) found.

The shape of the southern erosional wall is relatively round, which could explain why larger approach angles of the wind could be steered, realigned, and accelerated into the notch. It may even be argued that during south-westerly winds the orientation of the notch at the southern erosional wall is more south-west orientated than the 280N that was stated to be the notch orientation, allowing stronger southerly winds to enter the notch. Figure 5.4 shows the orientation used in this study (orange) and the orientation of the southern erosional wall (green), which is much more southwest orientated. Since the northern erosional wall is much more angular, it would be possible to confirm this theory by conducting measurements during north-westerly winds.

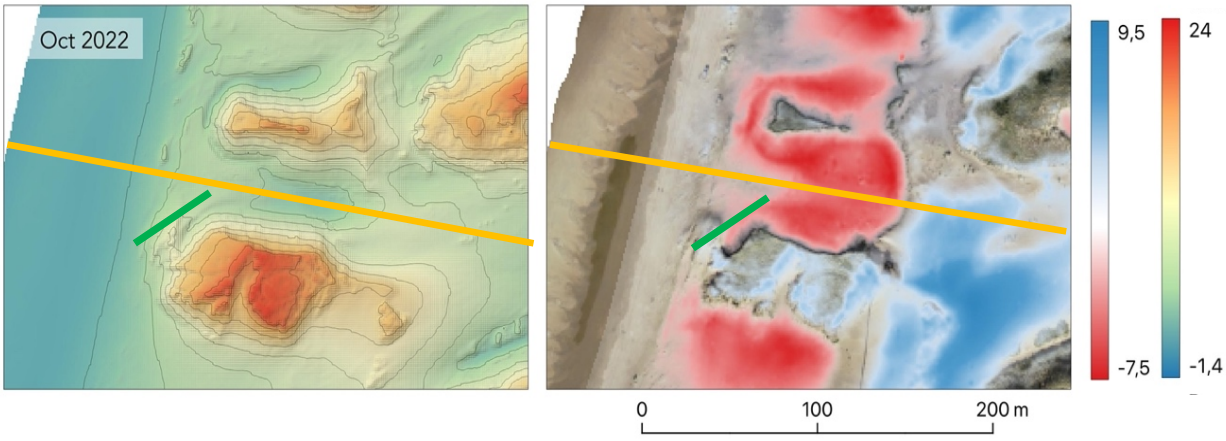

Figure 5.4: Overview of changes in the study area from just after the notch excavation in 2013 till the end of the field work. Left: DEM at the end of the fieldwork, right: differences between DEMs of just after excavation and at the end of the fieldwork. Orange: orientation notch used in study; green: local orientation southern erosional wall. Legend is in m MSL. Data used extracted from DOI 10.5281/zenodo.7010095

5.4 RECOMMENDATIONS

1. It is very useful to measure the wind characteristics and sediment transport with a smaller distance between the two sensors in an excavated notch or blowout, to determine whether a better correlation between wind characteristics and sediment transport can be found. Additionally, to determine whether turbulence (TKE) appears to be a better predictor at a smaller spatial distance in notches, like Ellis and Sherman (2022) found on beaches.

2. More measurements could be conducted under different wind conditions (e.g., westerly, and north westerly wind directions). This can then be used to examine the sediment transport patterns in the notch when the wind is parallel to the notch orientation and determine if the notch is indeed more effective in transporting sediment under those conditions as described in the literature. Additionally, examine if the same transport and wind patterns develop in the notch under oblique winds from the north-west, because the northern erosional wall has different shape (is more angular) than the southern erosional wall. Furthermore, it may be interesting to measure at additional points in the notch (e.g., in the deflation basin or on the depositional lobe) under the same conditions to see the pattern found evolve throughout the excavated notch.

3. If more measurements would be conducted, I would recommend installing a wind station that additionally measures the local amount of precipitation, air humidity and temperature. In addition, it may be useful to determine the moisture content of the sand. During this study, there were some differences between sediment transport rates while the wind conditions were similar. For example, on day 6 wind conditions were similar to those on days 7 and 8, however the amount of sediment transport measured was very different. Those differences might have been answered if data on precipitation, air humidity, and temperature (soil moisture) were available.

6. CONCLUSION

This study has provided several new insights and substantiated existing ideas regarding the properties and behaviour of aeolian sediment transport rates in the mouth of an excavated foredunes notch and how this depends on the weather conditions.

What is the correlation (relation) between sediment transport and different wind characteristics such as wind speed and Turbulent kinetic Energy?
How does the relation change for different temporal averaging intervals? (What is the best temporal averaging interval?)
A temporal averaging interval of 1-minute appeared to work well for this thesis (with this instrument set-up) when compromises were made between scatter, trend, and quantity of data. However, the trends which can be seen at the 5-minutes (and even for 10-seconds) averaging interval did not appear to be substantially different. The best temporal average interval may be dependent on the distance between measuring devices, since turbulence occurs on many spatial and temporal scales (Ellis & Sherman, 2022). Hence, the 1-minute is an appropriate temporal averaging interval for this setup with this accuracy.

What is the relation between sediment transport and different wind characteristics (wind speed and TKE)?
In this study, wind speed gave a much better the best correlation for sediment flux than the TKE. In general, sediment transport rates increase with increasing wind speed. When the wind reaches a certain threshold (generally between 3 and 5 m/s), sediment transport starts and increases in a roughly linear fashion with wind speed (slope between 15 and 30). The trend line of day 5 (Saltation Intensity [cnts/s] = 15.4 * U[m/s] – 48.3) provides a reasonably accurate prediction for sediment transport on other days but has its limitations. On the other hand, the relationship between TKE and sediment transport rates is scattered and not consistent for different locations and under different wind conditions.

What is the relation between coefficient of variation of the wind (CVk) and sediment transport rates? And the coefficient of variation of the sediment transport (CV)?
There is no clear trend between the CVk and sediment transport. In general, for low saltation intensities (smaller than 50 cnts/s) the CVk was really scattered and showed a large spread (between 0 and 700 %), whereas for high transport values (larger than 50 cnts/s) the spread and average value of the CVk were lower (smaller than 50 %).
Generally, the fluctuations in wind (CVk) also generate more fluctuations in sediment transport (CV). However, the CVk tended to be larger (between 0 and 450% for days with high transport rates, day 4, 5 and 9) than the CV (between 0 and 120% for days with high transport rates, day 4, 5 and 9).

What is the spatial variation of sediment flux in the notch mouth as a function of wind approach angle?
Under very oblique winds (angle larger than 50 degrees, from south-west in this thesis) the transport rates were highest at the first erosional wall it encounters (here southern erosional wall). The wind recorded there had highest wind speeds, the lowest turbulence (TKE) and the wind direction was altered most. Oblique winds do not move as a uniform sheet through the

notch: it is steered along the southern erosional wall, while in the middle and north of the notch the wind is less steered and becomes more turbulent.

Even though the wind became more turbulent and had relative lower wind speeds (than the approach wind speed) when the approach wind was very oblique (>50 degree, for example, on days 5 and 9), it was still realigned to the notch orientation and capable of moving large quantities of sediment. This is in contrast with most the literature, that found that when the angle was larger than 50 degrees, the wind would no longer enter the notch and transport sediment through it. This deviation from literature may be due to the roundness of the southern erosional wall is very rounded, making the orientation of the notch to be locally more southwest-northeast oriented than west-east allowing oblique winds from the southwest to enter the notch.

7. REFERENCES

Anthony, E. J. (2008). Shore processes and their palaeoenvironmental applications. *Elsevier*.

Arens, S. M. (1996). Rates of aeolian transport on a beach in a temperate humid climate. *Geomorphology*, *17*(1-3 SPEC. ISS.), 3–18. https://doi.org/10.1016/0169-555x(95)00089-n.

Arens, S. M. (1999). Evaluatie dynamisch zeereep beheer - vergelijking situatie 1988 en 1998 . *Ministerie van Verkeer En Waterstaat, Rijkswaterstaat, Dienst Weg- En Waterbouwkunde (RWS, DWW), in Dutch.*

Arens, S. M. , & Geelen, L. H. W. T. (2001). *Geomorfologie en regeneratie van duinvalleien; het Van Limburg Stirumproject als voorbeeld.*

Arens, S. M., Löffler, M. A. M., & Nuijen, E. M. (2007). *Evaluatie Dynamisch Kustbeheer Friese Waddeneilanden*.

Arens, S. M., Mulder, J. P. M., Slings, Q. L., Geelen, L. H. W. T., & Damsma, P. (2013). Dynamic dune management, integrating objectives of nature development and coastal safety: Examples from the Netherlands. *Geomorphology*, *199*, 205–213. https://doi.org/10.1016/j.geomorph.2012.10.034

Arens, S. M., Slings, Q., & de Vries, C. N. (2004). Mobility of a remobilised parabolic dune in Kennemerland, The Netherlands. *Geomorphology*, *59*(1–4), 175–188. https://doi.org/10.1016/j.geomorph.2003.09.014.

Arens, S. M., & Wiersma, J. (1994). The Dutch Foredunes: Inventory and Classification. In *Source: Journal of Coastal Research* (Vol. 10, Issue 1). Winter.

Baas, A. C. W. (2008). Challenges in aeolian geomorphology: Investigating aeolian streamers. *Geomorphology*, *93*(1–2), 3–16. https://doi.org/10.1016/j.geomorph.2006.12.015.

Baas, A. C. W., & Sherman, D. J. (2005). Formation and behavior of aeolian streamers. *Journal of Geophysical Research: Earth Surface*, *110*(3). https://doi.org/10.1029/2004JF000270.

Baas, A. C. W., & Sherman, D. J. (2006). Spatiotemporal variability of aeolian sand transport in a coastal dune environment. *Journal of Coastal Research*, *22*(5), 1198–1205. https://doi.org/10.2112/06-0002.1

Barchyn, T. E., & Hugenholtz, C. H. (2013). Reactivation of supply-limited dune fields from blowouts: A conceptual framework for state characterization. *Geomorphology*, *201*, 172–182. https://doi.org/10.1016/j.geomorph.2013.06.019

Bate, G., & Ferguson, M. (1996). Blowouts in coastal foredunes. In *Landscape and Urban Planning* (Vol. 34).

Bauer, B. O. et al. (1988). Event detection and conditional averaging in unsteady aeolian systems". . *Journal of Arid Environments* , 345–375.

Bauer, B. O., & Davidson-Arnott, R. G. D. (2002). *A general framework for modeling sediment supply to coastal dunes including wind angle, beach geometry, and fetch effects*. www.elsevier.com/locate/geomorph.

Bauer, B. O., Davidson-Arnott, R. G. D., Hesp, P. A., Namikas, S. L., Ollerhead, J., & Walker, I. J. (2009). Aeolian sediment transport on a beach: Surface moisture, wind fetch, and mean transport. *Geomorphology*, *105*(1–2), 106–116. https://doi.org/10.1016/j.geomorph.2008.02.016.

Bosma, J. (2020). *The Properties and Behaviour of Aeolian Streamers in a narrow sandy beach-dune system*.

Butterfield, G. R. (1993). Sand transport response to fluctuating wind velocity. *Turbulence: Perspectives on Flow and Sediment Transfer.*

Carter, R. W. G., Hesp, P. A. , & Nordstrom, K. F. (1990). *Erosional landforms in coastal dunes.*

Chapman, C. A., Walker, I. J., Hesp, P. A., Bauer, B. O., & Davidson-Arnott, R. G. D. (2012). Turbulent Reynolds stress and quadrant event activity in wind flow over a coastal foredune. *Geomorphology*, *151–152*, 1–12. https://doi.org/10.1016/j.geomorph.2011.11.015.

Chepil, W. S. (1957). "Width of field strips to control wind erosion". SoilConditions That Influence Wind Erosion. . *US Dept.of Agriculture*, *1185*, 40.

Clemmensen, L. B., Hansen, K. W. T., & Kroon, A. (2014). Storminess variation at Skagen, northern Denmark since AD 1860: Relations to climate change and implications for coastal dunes. *Aeolian Research*, *15*, 101–112. https://doi.org/10.1016/j.aeolia.2014.09.001.

Cooper, W. S. (1958). *Coastal SandDunes of Oregon and Washington.*

Corenblit, D., Baas, A., Balke, T., Bouma, T., Fromard, F., Garófano-Gómez, V., González, E., Gurnell, A. M., Hortobágyi, B., Julien, F., Kim, D., Lambs, L., Stallins, J. A., Steiger, J., Tabacchi, E., & Walcker, R. (2015). Engineer pioneer plants respond to and affect geomorphic constraints similarly along water-terrestrial interfaces world-wide. *Global Ecology and Biogeography*, *24*(12), 1363–1376. https://doi.org/10.1111/geb.12373.

Davidson-Arnott, R. G. D., & Bauer, B. O. (2009). Aeolian sediment transport on a beach: Thresholds, intermittency, and high frequency variability. *Geomorphology*, *105*(1–2), 117–126. https://doi.org/10.1016/j.geomorph.2008.02.018.

De Vries, S., van Thiel de Vries, J. S. M., van Rijn, L. C., Arens, S. M., & Ranasinghe, R. (2014). Aeolian sediment transport in supply limited situations. *Aeolian Research*, *12*, 75–85. https://doi.org/10.1016/j.aeolia.2013.11.005.

De Winter, R. C., Gongriep, F., & Ruessink, B.G.,. (2015). Observations and modeling of alongshore variability in dune erosion at Egmond aan Zee, the Netherlands. . *Coastal Eng.* , 167-175.

De Winter, W., van Dam, D. B., Delbecque, N., Verdoodt, A., Ruessink, B. G., & Sterk, G. (2018). Measuring high spatiotemporal variability in saltation intensity using a low-cost Saltation Detection System: Wind tunnel and field experiments. *Aeolian Research*, *31*, 72–81. https://doi.org/10.1016/j.aeolia.2017.11.003.

Delgado-Fernandez, I. (2010). A review of the application of the fetch effect to modelling sand supply to coastal foredunes. In *Aeolian Research* (Vol. 2, Issues 2–3, pp. 61–70). https://doi.org/10.1016/j.aeolia.2010.04.001.

Ellis, J. T., & Sherman, D. J. (2022). Cross-wavelet analysis of coherent wind and saltation events. *Earth Surface Processes and Landforms*. https://doi.org/10.1002/esp.5493

Ellis, J. T., Sherman, D. J., Farrell, E. J., & Li, B. (2012). Temporal and spatial variability of aeolian sand transport: Implications for field measurements. *Aeolian Research*, *3*(4), 379–387. https://doi.org/10.1016/j.aeolia.2011.06.001.

Gares, P. A. , & Nordstrom, K. F. (1995). A Cyclic Model of Foredune Blowout Evolution for a Leeward Coast : Island Beach , New Jersey . *Annals of the Association of Amercan Geographers*, 1–20.

Gares, P. A., Finn, C., Davidson-Arnott, R. G. D., Bauer, B. O., Sherman, D. J., Carter, R. W. G., Jackson, D. W. T., & Nordstrom, K. F. (1996). Alongshore Variations in Aeolian Sediment Transport: Carrick Finn Strand, Ireland. In *Source: Journal of Coastal Research* (Vol. 12, Issue 3).

Gillette, D. A., Hardebeek, E., & Parker, J. (1997). Large-scale variability of wind erosion mass flux rates at Owens Lake 2. Role of roughness change, particle limitation, change of threshold friction velocity, and the Owen effect. *Journal of Geophysical Research Atmospheres*, *102*(22). https://doi.org/10.1029/97jd00960.

Gillette, D. A., Herbert, G., Stockton, P. H., & Owen, P. R. (1996). Causes of the fetch effect in wind erosion. *Earth Surface Processes and Landforms*, *21*(7), 641–659. https://doi.org/10.1002/(SICI)1096-9837(199607)21:7<641::AID-ESP662>3.0.CO;2-9.

Hesp, P. (2002). *Foredunes and blowouts: initiation, geomorphology and dynamics*. www.elsevier.com/locate/geomorph.

Hesp, P. A. , & Hyde, R. (1996). Flow dynamics and geomorphology of a trough blowout. . *Sedimentology*, 505–525.

Hesp, P. A., & Pringle, A. (2001). Wind Flow and Topographic Steering within a Trough Blowout. In *Source: Journal of Coastal Research*. https://www.jstor.org/stable/25736325.

Hesp, P. A., & Walker, I. J. (2012). Three-dimensional æolian dynamics within a bowl blowout during offshore winds: Greenwich Dunes, Prince Edward Island, Canada. *Aeolian Research*, *3*(4), 389–399. https://doi.org/10.1016/j.aeolia.2011.09.002.

Hillen, R., & Roelse, P. (1995). Dynamic preservation of the coastline in the Netherlands. *Journal of Coastal Conservation* , 17–28.

Jungerius, P. D., Koehler, H., Kooijman, A. M., Mücher, H. J., & Graefe, U. (1995). Response of vegetation and soil ecosystem to mowing andsod removal in the coastal dunes 'Zwanenwater', the Netherlands. *Journal of Coastal Conservation* , 3–16.

Jungerius, P. D., Witter, J. v, & van Boxel, J. H. (1991). The effects of changing wind regimes on the development of blowouts in the coastal dunes of The Netherlands. In *Landscape Ecology* (Vol. 6, Issue 1). SPB Academic Publishing bv.

Jungerius, P., & van der Meulen, F. (1989). *THE DEVELOPMENT OF DUNE BLOWOUTS, AS MEASURED WITH EROSION PINS AND SEQUENTIAL AIR PHOTOS* (Vol. 16).

Klijn, J. A. ,. (1981). Nederlandse kustduinen - geomorfologie en bodems. . *Ph.D. Thesis, Landbouwhogeschool, Wageningen*.

Kuipers, M. , Arens, B. , & Ruessink, G. ,. (2016). Grootschalig herstel van stuivende duinen. . *De Levende Natuur* , 89–93.

Luijendijk, A. , de Vroeg, H. , Swinkels, C. , & Walstra, D. J. ,. (2011). Coastal response on multiple scales: a pilot study on the IJmuiden port. . *Coastal Sediments.*, 602-615.

Miller, T. E. (2015). Effects of disturbance on vegetation by sand accretion and erosion across coastal dune habitats on a barrier island. *AoB PLANTS*, *7*(1). https://doi.org/10.1093/aobpla/plv003.

Minh Nguyen, D. (2022). *WIND FLOW DYNAMICS AND SAND TRANSPORT THROUGH EXCAVATED FOREDUNE NOTCHES*.

Nickling, W. G., & Neuman, C. M. (2009). Aeolian sediment transport. . *Geomorphology of Desert Environments*, 517–555.

Nordstrom, K. F. 1, & Arens, S. M. (1998). The role of human actions in evolution and management of foredunes in The Netherlands and New Jersey, USA. *Journal of Coastal Conservation 4*, 169–180.

Pease, P., & Gares, P. (2013). The influence of topography and approach angles on local deflections of airflow within a coastal blowout. . *Earth Surface Processes and Landforms*, 1160-1169.

Petersen, P. S., Hilton, M. J., & Wakes, S. J. (2011). Evidence of aeolian sediment transport across an Ammophila arenaria-dominated foredune, Mason Bay, Stewart Island. *New Zealand Geographer*, *67*(3), 174–189. https://doi.org/10.1111/j.1745-7939.2011.01210.x.

Pye, K., Blott, S. J., & Howe, M. A. (2014). Coastal dune stabilization in Wales and requirements for rejuvenation. *Journal of Coastal Conservation*, *18*(1), 27–54. https://doi.org/10.1007/s11852-013-0294-8.

Ruessink, B. G., Arens, S. M., Kuipers, M., & Donker, J. J. A. (2018). Coastal dune dynamics in response to excavated foredune notches. *Aeolian Research*, *31*, 3–17. https://doi.org/10.1016/j.aeolia.2017.07.002.

Schwarz, C. , Brinkkemper, J. , & Ruessink, G. (2018). Feedbacks between Biotic and Abiotic Processes Governing the Development of Foredune Blowouts. *Journal of Marine Science and Engineering*, 2.

Sherman, D. J., Houser, C., Ellis, J. T., Farrell, E. J., Li, B., Davidson-Arnott, R. G. D., Baas, A. C. W., & Maia, L. P. (2013). Characterization of aeolian streamers using time-average videography. *Journal of Coastal Research*, *165*, 1331–1336. https://doi.org/10.2112/si65-225.1.

Smyth, T. A. G., & Hesp, P. A. (2016). Numerical modelling of turbulent flow structures in a trough blowout. *Journal of Coastal Research*, *1*(75), 328–332. https://doi.org/10.2112/SI75-066.1.

Smyth, T. A. G., Jackson, D., & Cooper, A. (2014). Airflow and aeolian sediment transport patterns within a coastal trough blowout during lateral wind conditions. *Earth Surface Processes and Landforms*, *39*(14), 1847–1854. https://doi.org/10.1002/esp.3572.

Spies, P. J., McEwan, I. K., & Butterfield, G. R. (2000). One-dimensional transitional behaviour in saltation. *Earth Surface Processes and Landforms*.

Van Boxel, J. H., Jungerius, P. D., Kieffer, N., & Hampele, N. (1997). Ecological effects of reactivation of artificially stabilized blowouts in coastal dunes. *Journal of Coastal Conservation* , 57–62.

Van Boxel, J. H., Sterk, G., & Arens, S. M. (2004). Sonic anemometers in aeolian sediment transport research. *Geomorphology*, *59*(1–4), 131–147. https://doi.org/10.1016/j.geomorph.2003.09.011.

Van der Laan, D., van Tongeren, O. F. R., van der Putten, W. H., & Veenbaas, G. (1997). Vegetation development in coastal foredunes-179. In *Journal of Coastal Conservation* (Vol. 3).

Van Kuik, N., de Vries, J., Schwarz, C., & Ruessink, G. (2022). Surface-area development of foredune trough blowouts and associated parabolic dunes quantified from time series of satellite imagery. *Aeolian Research*, *57*. https://doi.org/10.1016/j.aeolia.2022.100812.

Veer, M. A. C., & Kooijman, A. M. (1997). Effects of grass-encroachment on vegetation and soil in Dutch dry dune grasslands. In *Plant and Soil* (Vol. 192). Kluwer Academic Publishers.

Walker, I. J. , Davidson-Arnott, R. G. , Bauer, B. O. , & Hesp, P. A. ,. (2017). Scale-dependent perspectives on the geomorphology and evolution of beach-dune systems. . *Earth-Science Reviews*, 220-253.

Wyngaard, J. C. (1992). Atmospheric Turbulence. *Annual Review of Fluid Mechanics* , 205–234.

Zarnetske, P. L., Ruggiero, P., Seabloom, E. W., & Hacker, S. D. (2015). Coastal foredune evolution: The relative influence of vegetation and sand supply in the US Pacific Northwest. *Journal of the Royal Society Interface*, *12*(106). https://doi.org/10.1098/rsif.2015.0017.